DOE/NASA/2593-24
NASA TM-81708

Gas-Turbine Critical Research and Advanced Technology Support Project: FY 1979 Annual Report

John S. Clark, Philip E. Hodge, Carl E. Lowell, David N. Anderson, and Donald F. Schultz
National Aeronautics and Space Administration
Lewis Research Center

March 1981

Prepared for
U.S. DEPARTMENT OF ENERGY
Fossil Energy
Office of Coal Utilization

DOE/NASA/2593-24
NASA TM-81708

Gas-Turbine Critical Research and Advanced Technology Support Project: FY 1979 Annual Report

John S. Clark, Philip E. Hodge, Carl E. Lowell,
David N. Anderson, and Donald F. Schultz
National Aeronautics and Space Administration
Lewis Research Center
Cleveland, Ohio 44135

March 1981

Work performed for
U.S. DEPARTMENT OF ENERGY
Fossil Energy
Office of Coal Utilization
Washington, D.C. 20545
Under Interagency Agreement DE-AI01-77ET10350

SUMMARY

This report summarizes the technical progress made during FY 1979 to provide a critical-technology data base for utility gas-turbine systems capable of burning coal-derived fuels. Coal-derived fuels present two major problems to utility gas turbines. First, they are typically high in organically bound nitrogen, which is converted in the combustion process to oxides of nitrogen (NO_x). Second, they contain trace-metal contaminants that can lead to hot corrosion and/or fouling in turbine hot sections.

A combustion task is under way to address the first problem. A literature survey of coal-derived fuel properties was completed and a NO_x emission model was developed. A two-stage test rig was designed and tests were run to study the conversion of fuel-bound nitrogen to NO_x. Catalytic combustion tests were also initiated to evaluate the feasibility of using heavy fuel in catalytic combustors.

To address the second problem, a statistically designed series of hot-corrosion burner rig tests were conducted to measure the corrosion rates of typical gas-turbine alloys with several fuel contaminants. The resultant data have been correlated into a hot-corrosion-life prediction model. This model was extended to longer times in 1979. Another approach to solving the hot-corrosion problem is to use a fuel additive that inhibits hot corrosion. Barium and strontium were identified as being particularly beneficial fuel additives. Still another approach to preventing hot corrosion is to protect the hot components with a coating. Ceramic thermal-barrier coatings offer potential corrosion resistance as well as thermal protection. Several advanced thermal-barrier coatings have demonstrated promising hot-corrosion resistance. Coating life was found to be a strong function of coating thickness.

Systems studies were also conducted to help integrate and guide the technological efforts. An Analytical Study of thermal-barrier coatings used in conjunction with low critical alloys was completed. A study of thermal-barrier coatings used in a combined cycle system in which the stack temperature was maintained above the acid corrosion temperature was also studied.

INTRODUCTION

The Critical Research and Advanced Technology Support Project (CRT) is directed toward providing a critical-technology data base to support the development of gas-turbine systems capable of burning coal-derived fuels. The CRT project was begun by the NASA Lewis Research Center and the ERDA Office of Fossil Energy on June 30, 1977. A 40-month period of performance was planned. Upon creation of the Department of Energy on October 1, 1977, the project was assigned to the DOE Division of Power Systems, which has been renamed the Office of Coal Utilization. This report summarizes the technical progress made during.

The focus of the effort in this project has been on "critical" technologies - those problems that must be resolved before coal-derived fuels can be considered viable for use in gas turbines. Two technologies have been identified for inclusion in this effort: combustion and materials. Emphasis in the combustion task is on reducing both thermal and fuel-bound NO_x emissions. Emphasis in the materials task is on trace-metal contaminants in coal-derived fuels, which can lead to unacceptable hot corrosion in the turbine hot section. Several approaches to solving the materials problem

are being investigated, including developing a hot-corrosion-life model and using fuel additives or protective coatings. Systems studies were made to help integrate and guide the materials and combustion tasks.

The technical objectives of the CRT project are:

(1) To develop combustor concepts that will use coal-derived fuels in an environmentally acceptable manner
(2) To develop a hot-corrosion data base for materials exposed to combustion products of coal-derived fuels and to correlate these data in a hot-corrosion-life prediction model
(3) To develop ceramic coatings that have acceptable life in coal-derived-fuel combustion products
(4) To study the trade-offs among various gas-turbine technologies, operating conditions, and component designs

The following sections discuss the purpose of each task, our approach to it, and its present status. A detailed discussion of results is included where appropriate.

TASK 1.0 - SYNCRUDE AND SYNFUEL CHARACTERIZATION AND COMBUSTION STUDIES

The objectives of this task are (1) to establish a data base of the properties of coal-derived fuels (subtask 1.1) and (2) to evolve combustion technology so that these fuels can be used in utility industrial gas turbines with minimum NO_x pollution (subtasks 1.2, 1.3, and 1.4). This task is also planned to provide data to aid in establishing fuel specifications for advanced gas-turbine systems buring coal-derived fuels in an environmentally acceptable manner. Each subtask is described in the following sections.

SUBTASK 1.1 - SYNCRUDE AND SYNFUEL CHARACTERIZATION

The objective of this subtask is to assemble in a systematic manner existing data regarding physical, chemical, elemental composition and structural characteristics of synthetic fuels derived from coal. Efforts consist of literature surveys and data evaluation of coal-derived liquid and low-Btu gas fuel properties. Survey results are being completed in the following categories:

1. Descriptive material in which fuel properties of greatest interest, as well as the coal conversion refining processes, are described;
2. Data base tables in which fuel properties, a bibliography of reference sources and fossil energy contract numbers are tabulated;
3. Summary material which includes fuel property data tables by distillate categories, data plots indicating trends in synfuel properties irrespective of process type and identification of fuel characterization data which is required but not available in the literature.

The survey emphasizes, but is not limited to, the development and upgrading of DOE-sponsored pilot plants. NASA fuel processing or characterization is not included as part of this effort.

A literature survey was conducted in 1978 and has been published as DOE/NASA/2593-79/8 (ref. 1). An update of the survey will be published in 1981. Summary data plots from the report for liquid fuels are included as figures 1 to 3. These figures indicate fuel property trends common to several processes.

Figure 1 shows the trend of weight percent hydrogen with API gravity of the product. Figure 2 shows how weight percent nitrogen contained in the fuel varies with weight percent hydrogen. As hydrogenation severity of the process increases, fuel bound nitrogen levels decrease with conversion of fuel nitrogen to ammonia. Figure 3 shows the variation of heat of combustion with weight percent hydrogen.

Low-Btu gases produced from air-blown gasifiers contain large amounts of inerts such as nitrogen and carbon dioxide as well as combustibles consisting of H_2, CO and a small amount of methane. Since the gross volumetic heating values of H_2+CO are nearly identical, approximately 322 Btu per standard cubic foot, the heating value of a low Btu gas can be estimated if the volume of inerts is known. A plot of this relationship is shown in figure 4.

SUBTASK 1.2 - NO_x EMISSION MODELING

The objective of this subtask is to analytically determine, through computer modeling, the effects of combustor operating conditions and geometry on the conversion of fuel bound nitrogen into oxides of nitrogen (NO_x). Several approaches have been pursued to model fuel bound nitrogen conversion. Initial attempts emphasized modification of an existing well-stirred reactor model. Results, while indicating trends consistent with experimental data, did not provide acceptable results under rich burning (stoichiometries greater than 1) conditions. Thus, subsequent efforts have emphasized evolution of a chemical kinetics combustor model consisting of a two-stage, adiabatic, perfectly stirred reactor. Burning stages consist of a rich primary burning stage, air dilution, and lean second stage burning. Computations are proceeding for:

1. Propane-air mixtures for varying amounts of added fuel-bound nitrogen
2. Toluene-air mixtures for varying amounts of added fuel-bound nitrogen
3. Propane/toluene-air mixtures (11 percent hydrogen in fuel) for varying amounts of added fuel-bound nitrogen.

A 57-reaction chemical mechanism is being used for propane oxidation. The effects of operating conditions on carbon monoxide are also being examined.

Propane air computations for varying levels of fuel bound nitrogen have been completed and presented in reference 2. Toluene air computations are nearly complete. Publication of these results is planned at the 1981 ASME Gas Turbine Conference.

In this study the effects of operating conditions on pollutant formation in two-stage combustion have been predicted for various propane-air mixtures. Various amounts of fuel-bound nitrogen, up to 2 percent by weight as nitrogen atoms, were used. The product gases of the primary stage are assumed to be diluted by adding air in the second stage to an overall equivalence ratio of either 0.7 or 0.5. The computed results were then compared with experimental data. The important results of this work may be summarized as follows:

1. Minimum NO_x formation occurs in general when the primary zone equivalence ratio is between 1.4 and 1.5. However, for this range of values, the CO formation is at its highest level.
2. The percentage conversion of fuel bound nitrogen to NO_x is greatest for small percentages of FBN and decreases as FBN content is raised above 0.5 percent by weight.

3. The final concentrations of NO_x and CO are significantly reduced by additional secondary dilution from an equivalence ratio of 0.7 to 0.5. The extra dilution lowers the secondary reaction temperature by about 300 K and thus suppresses all secondary stage NO_x reactions. Therefore, the change in NO_x concentration due to the added dilution is strictly an effect of more dilution to the primary mixture. For CO, however, the final CO concentration is always a combined result of diluting the primary mixture and secondary-zone chemical reaction. This is because temperature appears to have very little effect on CO destruction chemistry in the present model.
4. For secondary dilution to an equivalence ratio of 0.5, NO_x concentration appears to be independent of secondary residence time, over the range tested. This is because of the suppression of NO_x reactions due to the low secondary zone reaction temperatures. For secondary dilution of rich primary mixtures to an equivalence ratio of 0.7, NO_x forms in the secondary zone due to chemical reaction. Therefore, NO_x concentration increases with increasing secondary residence time for these rich primary mixtures only. Only in this region is chemical reaction important in the secondary zone. The final CO concentration always decreases with increasing secondary residence time because, in the present model, chemical reaction to destroy CO is not strongly affected by temperature.
5. Final NO_x and CO concentrations show only minor dependence on primary zone residence time.
6. Comparison of computed results with limited experimental data indicates that there is good agreement in trends between the prediction and the experiment. The quantitative agreement steadily improves as the primary equivalence ratio increases. For the values of greatest interest (Φ_p=1.4) the agreement between theory and experiment is within + 50 percent. Apparently, effects of experimental heat transfer losses and mixing non-homogeneity are less for these rich primary mixtures. These last two factors were not considered in the theoretical combustion model.

SUBTASK 1.3 - FLAME TUBE EXPERIMENTS

The objective of this subtask is to experimentally evolve fundamental combustion concepts for minimizing the converson of fuel-bound nitrogen to NO_x, determine achievable baseline levels of fuel-bound nitrogen conversion to NO_x and provide verification of the subtask 1.2 analytical model. Fundamental flame tube combustion experiments, including two-stage combustion with independent airflow control to each stage, have been conducted and combustion and emissions data have been recorded. Test series for ranges of stoichiometric burning conditions were conducted with gaseous propane fuel, propane with pyridine addition, toluene fuel, toluene-propane blends, toluene-propane-pyridine mixtures and with SRC-II naphtha and SRC-II mid-distillate liquid fuels.

The technical effort for this subtask has been completed and the results published in reference 3. A schematic drawing of the test rig, illustrating flow, geometric and measurement parameters of interest is contained in figure 5. Photographs of the test rig and combustion sections are contained in figures 6 and 7, respectively. In operations, air at

670 K and 0.48 mPa were premixed with fuel, burned at primary equivalence ratios of 0.5 to 2.0 and secondary equivalence ratios ranging from 0.5 to 0.7. Fuel blends were proportioned to vary hydrogen composition from 9.0 to 18.3 percent and fuel nitrogen composition form 0 to 1.5 percent. Distillates of coal syncrude produced by the SRC-II process were also tested, and the results compared to the data obtained with the propane-toluene-pyridine fuel blends. In addition to oxides of nitrogen, the exhaust gas was sampled for carbon monoxide, carbon dioxide, unburned hydrocarbons, and smoke. Among the more significant results obtained were the following:

1. Rich-lean two-stage combustion successfully reduces fuel-bound nitrogen to NO_x conversion. Conversion rates of less than 10 percent can be achieved at optimum primary burning zone conditions as shown in figure 8. Illustrated are plots of percent fuel nitrogen conversion to NO_x as a function of primary zone equivalence ratio, for three fuel nitrogen concentrations. For lean burning conditions, conversion of fuel nitrogen to NO_x is significant - 35 to over 60 percent. For rich burning conditions significant amounts of fuel nitrogen are converted to elemental nitrogen with correspondingly lower conversion to NO_x.
2. The optimum primary equivalence ratios ranged between 1.4 and 1.7. The optimum secondary equivalence ratio for these tests was about 0.5. These values resulted in minimum NO_x production at acceptable combustion efficiencies.
3. Fuel hydrogen content had some effect on the optimum primary equivalence ratio. Decreased hydrogen content shifted the optimum primary operating conditions to richer values, as illustrated in figure 8(b).
4. Increased fuel nitrogen levels reduced the percentage of fuel nitrogen to NO_x conversion. Exhaust NO_x levels, however, always increased with additional fuel nitrogen.
5. Rich burning combustion systems, while controlling fuel nitrogen conversion to NO_x may also produce larger smoke concentrations than lean burning systems. Sufficient data to quantify this effect were not obtained in these tests which were confined to low pressure operation of five atmospheres or less, due to test facility limitations. In subtask 1.4 testing, which will be conducted at high pressure conditions, rich burn smoke levels will be more fully explored.

SUBTASK 1.4 - COMBUSTOR SECTOR TESTS

The objective of this subtask is to evolve and evaluate experimental combustors capable of burning coal-derived fuels in an environmenally acceptable manner. Combustor testing will be conducted at representative industrial/utility gas-turbine temperatures and pressures over an entire simulated load range from engine cranking to peak power. Distillate fuels, heavy oils, doped heavy oil fuels and coal-derived fuels (as available) will be tested. Combustion efficiency, liner temperatures, exit temperature distributions, gaseous emissions, smoke levels, and deposit characteristics will be investigated. Tests will be run with thermal-barrier coatings on the inside of the combustor liner to determine their effects on performance and durability. Various levels of combustor technology will be evaluated to assess the degree of complexity required to achieve adequate emissions and performance. Existing combustor hardware, advanced combustor

concepts and combustion concepts currently beyond present state-of-the-art, will be tested. This testing should be completed in early 1981.

TASK 2.0 - LONG-LIFE MATERIALS

CORROSION RESISTANCE

Coal-derived fuels contain varying amounts of trace metals, some of which may lead to hot corrosion or excessive deposition and fouling in the gas turbine hot section. Task 2.0 was undertaken to contribute to the evaluation and prevention of hot corrosion and to determine the extent and possible consequences of deposition and fouling.

SUBTASK 2.1 - FUEL CORROSIVITY PREDICTION

Subtask 2.1 was planned to evaluate the resistance of high-strength superalloys to potential fuel impurities using doped clean fuels and coal-derived liquids. This work was also planned to evaluate additive techniques for the reduction of the corrosive effects of such fuel impurities.

SUBTASK 2.1.1 - DOPED-FUEL TESTS

These doped-fuel tests were run with simulated coal-derived fuels. In these tests, selected contaminants were added to a clean fuel (1) to isolate the corrosion effects of a given contaminant and its concentration and (2) to determine the interrelationships of time, temperature, and corrodent on hot corrosion. In FY 1979, three major activities were pursued in this subtask. The first area of effort was an evaluation of the data obtained on the 100 hour, high impurity level tests run in 1978. This information was incorporated into a model for hot corrosion as a function of time, temperature and impurity level. These efforts are summarized below. The second part of this subtask was the running of long time (400 hr), low impurity tests. The data from these tests is in the final stages of evaluation and will not be reported here. The third and final part of this subtask involves an evaluation of the effects of potential coal-derived liquid impurities on accelerated attack. This work was completed in FY 1979 and will be summarized below.

HOT CORROSION MODEL

The effects of potential impurities such as Na, K, Mg, Ca, and Cl, in coal-derived liquid fuels on accelerated corrosion of IN-100, U-700, IN-792, and Mar M-509 were investigated using a Mach 0.3 burner rig (fig. 9) for times to 200 hours in 1-hour cycles. These impurities were injected in combination as aqueous solutions into the combustor. Other variables were time, temperature, and fuel-to-air ratio. The experimental matrix was a central composite fractional factorial design divided into blocks to allow modification of the design as data was gathered. The extent of corrosion was determined by metal consumption. These data were fitted by non-linear regression analysis to the expression:

$$T = C_{Na}\, C_K\, C_{Ca}\, C_{Mg}\, C_{Cl}\, t^{B1}\, e^{B2+B3T+B4T^2}$$ (See Table I)

The time exponent B_1 was near 1.0 for the least corrosion resistant alloys, U-700 and IN-100; near 0.8 for the moderately resistant IN-792; and close to 0.5 for Mar M-509, the most corrosion resistant alloy. As anticipated, corrosion rapidly increased with increasing temperature (T). Corrosion increased with Na and K concentrations, while corrosion rates decreased somewhat as the Ca concentration increased for all alloys (fig. 10). Mg was beneficial for the Ni-base alloys, but had little effect on the Co-base alloys. Surprisingly, the effect of increasing Cl was to decrease the corrosion of all alloys. Little interaction among the dopants was noted. This work has been published as a NASA/DOE report (see ref. 4).

IMPURITY EFFECTS ON CORROSION

Other effects of potential coal-derived liquid fuel impurities on the hot corrosion of some selected nickel-, cobalt-, and iron-base alloys were also tested in a Mach 0.3 burner rig (ref. 5). The alloys tested were four nickel-base alloys, IN-100, IN-792, IN-738X, and U-700; one cobalt-base alloy; Mar M-509, and an iron base alloy; 304 stainless steel.

The combustion gases of the burner rig were doped by adding aqueous solutions of the potential fuel impurities. The temperature range was 700 to 900° C. The samples were heated for an hour at temperature, then cooled for six minutes in a high-velocity cool air stream and then the cycle repeated. The total number of cycles per test was 100. The elements added were sodium, potassium, vanadium, molybdenum, tungsten, phosphorus and lead. The baseline test was a simple addition of sodium, while the other elements were added in combination with the sodium and the results compared to the sodium-only values. As a result of these tests, it was determined that all of the elements caused enhanced corrosion under some conditions (fig. 11). The hot corrosion enhancement was determined to be due, at least in part, to the deposition of low-melting-point materials in combination with the normal sodium sulfate deposit. The effect of varying sodium-potassium ratio (fig. 12) was not large except at concentrations near zero sodium, in which case the hot corrosion was greatly depressed. However, some hot corrosion did take place with potassium only, even though the test was greater than 150° C below the melting point of the deposit: potassium sulfate. A report covering this work more fully has been published as a NASA/DOE report (ref. 2).

SUBTASK 2.1.2 - ADDITIVE TESTS

In FY 1978 barium was identified as an additive with great potential for reducing hot corrosion caused by sodium sulfate. However, the mechanism by which barium reduced or eliminated hot corrosion involved the deposition of a layer of barium sulfate. The object of the work in 1979 was to maintain the desirable inhibiting effects of barium while reducing the amount of deposition of the inert sulfate. Two approaches were evaluated. In the first, various elements were added with the barium. In the second, attempts were made to add the barium during only part of the exposure. As in the case of the doped fuel work, the tests were carried out in Mach 0.3 burner rigs and the alloys used were IN-100, U-700, IN-792, and Mar M-509.

The results of the elemental additions are summarized in Table II. In general, most of these additions resulted in increased hot corrosion, especially on IN-100, even though in some cases the apparent deposition rates decreased. The elemental addition which resulted in a substantial reduc-

tion in deposition (a factor of 2) and little increase in corrosion was silicon. Even here some slight increase in attack was noted in IN-100. Strontium was very effective in retaining corrosion resistance, but did not reduce the amount of deposition. It was evaluated in the other part of the program as an inhibitor both by itself and in conjunction with barium.

The results of the non-continuous application of the inhibitor are summarized in Table III. In brief, these data indicate that an addition of barium and/or strontium can be discontinued and the alkaline earth sulfate deposit will remain an effective barrier to hot corrosion for some time. In these tests, a 40-hour treatment was beneficial for more than forty additional hours. This would indicate that such an intermittent application approach could be used to prevent excessive build up of the inert sulfate while retaining the full hot corrosion resistance of the additive. This work is described in more detail in reference 6.

SUBTASK 2.1.3 - ACTUAL FUEL TESTS

Two actual fuel tests were completed in FY 1979: (1) a test of 184 hours duration using SRC-II naphtha; and (2) a test of 44 hour duration using a diesel fuel oil micronized coal mixture. The pertinent compositional information is shown in Tables IV and V.

The SRC-II naphtha tests were terminated when it was noted that no accelerated attack was occuring, as noted by weight change and microstructural evaluation. However, since the alkalai content was so low, no accelerated attack was expected. The microstructure of a typical bar is shown in figure 13. There was a heavy inert deposit whose phase and chemical analyses are shown in Table V. Only a small depletion zone and no measurable metal recession were found. As noted above, no accelerated corrosion was expected or found. Figure 14 shows the measured weight gains for the various specimens. A report covering this work is planned in FY 1980.

The micronized coal/diesel fuel oil test was terminated when the available fuel was expended. The results of this test indicate that no corrosion or erosion occurred, but there was massive deposition. The analysis of this test and a report covering this work is planned in FY 1980.

SUBTASK 2.2 - DEPOSITION AND FOULING

This subtask has two objectives: (1) to make thermodynamic predictions of the composition and dew points of deposits formed from the combustion of coal-derived fuels, and (2) to determine the potential for plugging of advanced cooling systems on airfoils in turbines operating on coal-derived liquids.

SUBTASK 2.2.1 - COMBUSTION PRODUCTS ANALYSIS

These tests are performed in a Mach 0.3 burner rig equipped with a special platinum target as shown schematically in figure 15. Three SRC-II distillate cuts, whose compositions are given in Table VI, were burned for periods of up to 6 hours each. The deposit collected on the platinum target was phase and chemically-analyzed, and compared to the predictions made based on the LeRC Complex Chemical Equiolibrium Calculation program (ref. 7). The deposit analysis and the predictions are shown in Tables VII and VIII. In general, the agreement between the predictions and the analyses is good, indicating that the program can be used to reliably predict

the type of depositions one would expect when burning coal-derived liquids. This work will be reported as a NASA/DOE report in 1980.

SUBTASK 2.2.2 - AIRFOIL COOLING HOLE PLUGGING

This subtask was undertaken to estimate the potential of cooling-hole plugging in the combustion environment of coal-derived fuels. Two airfoil cooling schemes were planned:

1. Film cooling - with relatively large coolant holes and high coolant velocity. This work was completed and reported earlier (ref. 8).
2. Transpiration cooling - with many small holes and low coolant velocity. It was planned that specimens from a DOE contractor would be tested in the Mach 0.3 rigs. However, in subsequent discussions involving DOE and their contractor, it was decided not to test this hardware.

SUBTASK 2.3 - THERMAL BARRIERS

This subtask is divided into three major elements. The first is aimed at determining the effects of operating parameters on thermal barrier coating life. This includes determining the effect of fuel-to-air mass ratio (and hence, hot gas temperature), the effect of temperature gradient through the thermal barrier, and the effect of bond coat or substrate temperature on overall thermal barrier coating system performance in a combustion environment generated by firing a clean fuel (jet A) doped to a fuel impurity equivalent of 5 ppm Na + 2 ppm V. The mode of failure and failure location of ZrO_2-type thermal barriers were analyzed on the basis of dew and melting points of the condensates from NA and/or V-containing combustion gases. The second element is aimed at improving the bond coat layer to provide better thermal barrier adherence via improved bond coat hot corrosion and oxidation resistance. The third element involves an experimental study of the reactions of thermal barrier coatings with potential fuel and air impurities. Powders of two thermal barrier coating materials were reacted with equivalent amounts of potential fuel, air and bond coat derived impurities. Results from these elements form the basis for analyzing the coating failure mechanisms and for developing more impuritytolerant thermal barrier coating systems.

SUBTASK 2.3.1 - ADVANCED THERMAL BARRIER COATINGS

In FY 1978, a number of ceramic thermal barrier coatings were identified in a hot corrosion burner rig test as having improved resistance to fuel and air impurities (ref. 9). The results of those tests indicated a need to establish a larger data base on how operating parameters affect thermal barrier coating system performance. These parameters include the effect of (a) oxide thickness on durability in doped combustion gases, (b) fuel-to-air ratio on overall performance, (c) substrate and bond coat temperature on useful life in oxidation or hot corrosion, (d) bond coat composition on thermal barrier life, and (e) surface temperature and temperature gradient through the thermal barrier coating on coating life. Two Mach 0.3 burner rig test series were initiated in FY 1979, to establish the effects of some of these variables on thermal barrier coating life.

In the first Mach 0.3 burner rig test, thermal barrier coating thickness and bond coat composition were variables. Coated specimens (IN-792) were tested in an eight-specimen test fixture in a manner similar to a previously reported test (ref. 9). Testing conditions were as follows: fuel-to-air mass ratio of 0.046, distance of specimen from the burner nozzle of 3.18 cm (1.25 in), gas calculated temperature of 1552° C (2825° F), ceramic surface temperature for a 15 mil yttria-stablized zirconia coated specimen of 843° C (1550° F) and fuel impurity equivalent level of 5 ppm Na and 2 ppm V. In these tests, the flux of impurities to the specimens, which is a function of the amount of impurities in the fuel and fuel usage, was 15 percent greater than in the prior tests (ref. 9) where the fuel-to-air ratio was 0.040. Also, the hot gas temperature was increased 180° C. The cyclic conditions such as length of exposure and inspection intervals were the same as in the previously referenced tests, except that now specimens were cooled when out of the flame, with an external blast of air in addition to the internal cooling air. In view of these changes, the test is more severe. The results are summarized in figure 16. The coating failure criteria was spallation of 1/4 of the coating area in the hot zone of the leading edge.

Based on a preliminary analysis of the results of these tests:

1. There appears to be a 3-to-4X improvement in the durability of both Ca_2SiO_4 and ZrO_2- based thermal barrier systems in the Na + V-doped combustion flame when the thermal barrier thickness is reduced to 0.012 cm from 0.038 cm. There is, of course, a proportional reduction in temperature drop through the thermal barrier coating for a reduction in thickness.
2. CoCrAlY bond coats appear to offer a 2-to-3X improvement in coating life compared to NiCrAlY bond coats for Ca_2SiO_4 thermal barrier coating systems.
3. The NiCrAlY bond coats, Ni-18Cr-12Al-0.3Y and Ni-31Cr-11Al-0.6Y, (from the bond coat optimization task) appear to improve thermal barrier coating system durability about 2X in Na + V-doped combustion gases compared to Ni-16Cr-6Al-.31Y.

In the second Mach 0.3 burner rig test, three yttria-stabilized zirconias and the $1.8CaO\text{-}SiO_2$ thermal barrier coatings were tested at three fuel-to-air mass ratios. The objectives of this effort were to determine how flame temperature (and thus combustion products) and temperature gradient through the thermal barrier coatings affect thermal barrier system performance in 5 ppm Na + 2 ppm V-doped combustion gases. Multiple specimen testing was similar to the previously referenced tests, except that 1/2" O.D. Waspaloy specimens were used for this test. The results of this test are summarized graphically in figure 17. Each data point represents the test results of two or more specimens. The criterion for coating failure was spallation of 1/4 of the coating area from the specimen leading edge where the substrate temperature was maintained at 1550° F. The time of spallation for Ca_2SiO_4 coated specimens in the trailing edge area were recorded also. The temperature of the ceramic surface was measured optically in this area and found to be 50° F higher than in the area facing the burner nozzle. Spallation of zirconia-based systems occurred at both the leading and trailing edge areas at about the same time. The data indicate that yttria-stabilized zirconia thermal barrier coatings are sensitive to changes in the fuel-to-air mass ratio. The Ca_2SiO_4 coating does not appear to be as sensitive to fuel-to-air ratio as zirconia, based on times-to-coating-failure at the hotter specimen trailing edge. Leading

edge failures of Ca_2SiO_4 coated specimens were not observed within the 1000-hour duration of these tests.

As the fuel-to-air mass ratio was changed from 0.039 to 0.049 the following occurred: the amount of fuel impurities increased 25 percent, the surface temperature of the ceramic was higher, and the temperature gradient throughout the coating was higher. Other possible effects of changing the fuel-to-air mass ratio were that new corrosive species might be formed or that the thermodynamic dew points of the condensates changed significantly. Completion of the analytical work and thermodynamic calculation of the dew points of the condensates should be helpful in determining which of the parameters that change as the fuel-to-air is altered affect coating performance.

In order to provide a basis for understanding and analyzing the failure of thermal barrier coating systems when exposed to dirty fuel combustion products, previous tests of the NASA-Lewis thermal barrier coating system ZrO_2-12Y_2O_3/NiCrAlY at Westinghouse (ref. 10), GE (ref. 11), and NASA-Lewis (ref. 9) have been reviewed. The test series carried out at NASA-Lewis was the focus of the analysis since the coating was exposed to all of the possible temperature conditions that were expected. Coating failure and failure location were explained (ref. 12) in terms of the thermodynamic dew points and melting points of the condensates and the temperature distributions within the coatings for these three series of tests.

The response in NASA-Lewis tests (ref. 9) of single ZrO_2-12w/o-Y_2O_3/Ni-16Cr-6Al-0.6Y coated air-cooled specimens to Mach 0.3 burner rig exposure with various levels of Na and V-fuel contamination is summarized in figure 18. This coating was originally developed for a clean fuel application (ref. 13). At the 0.5 ppm fuel equivalent sodium level, the coating survived 1300 1-hour cycles without spallation. Appreciable erosion, presumably due to carbon particles, was noted. At the 5 ppm fuel equivalent sodium level, the coating failed in a short time at a location outside the hot zone as shown in figure 19. With 0.2 and 2.0 ppm V, the coating failed in about 200 and 25 1-hour cycles, respectively. With vanadium in the combustion gases, failures occurred in the hot zone as shown in figure 20. When a fuel equivalent dopant level of 5 ppm Na + 2 ppm V was used, the coating also failed rapidly – in about 43 1-hour cycles. However, now the failure occurred both in the hot zone and out of the hot zone as shown in figure 20. The microstructure of the coating on this specimen after exposure is shown in figure 21, along with microstructure of the as-deposited coating. Here, as well as in the other tests, no bond coat corrosion was detected. In addition, coating failure in these tests occurred within the ceramic near the bond coat/oxide interface. This mode of failure is similar to failures observed in cyclic burner rig tests with clean fuels (ref. 12) and in mechanical tests (ref. 14).

The locations of the failures observed in these doped fuel tests were in qualitative agreement with thermodynamic predictions of condensate compositions and their dew points, melting points, and locations within the coating. These are summarized in Table IX. The most severe conditions for a porous plasma-spray-deposited ceramic coating such as ZrO_2-12w/o-Y_2O_3 occur when a corrosive liquid such as V_2O_5 or $Na_2V_2O_6$ can condense at the surface and completely permeate the coating. That is, the dew point T_{dp} is above the surface temperature, T_s, of the ceramic and the melting point, T_{mp}, is below the bond coat temperature, T_{bc}. This was the case with V_2O_5 formed in the 0.2 ppm, 2 ppm and 5 ppm Na + 2 ppm V tests and $Na_2V_2O_6$ formed in the 5 ppm Na + 2 ppm V test. The

problem with fuel or air impurities should not be as severe if the condensed combustion product is not reactive with the ceramic coating. If the melting point of the condensate is above the dew point (i.e., the condensate is a solid), or if the dew point is below the bond coat temperature, the fuel contaminant may be harmless. The fuel contaminant may also be harmless if the dew point is less than the surface temperature. With 5 ppm Na in the fuel, the dew point of the non-reactive Na_2SO_4 condensate was below the surface temperature in the hot zone. Failure occurred out of the hot zone where the dew point was above the surface temperature as illustrated in figure 22. With 0.5 ppm Na in the fuel, the dew point was below the bond coat temperature in the hot zone and below the surface temperature, but above the bond coat temperature elsewhere. Thus, this test was not more severe than an oxidation test.

SUBTASK 2.3.2 - BOND COAT OPTIMIZATION

The work in this subtask is aimed at improving the oxidation and corrosion resistance of the bond coating and the adherence of the thermal barrier coating. Three test methods were used to evaluate bond coatings. Two of the methods were cyclic furnace tests which were run to determine the durability of bond coatings alone (oxidation), and that of bond coatings used with thermal barrier coatings (endurance). The third method of evaluation was to test thermal barrier coating systems in a Mach 0.3 burner rig.

In endurance testing at 1012° C (1850° F), 22 bond coats were evaluated on B-1900 + Hf. The best bond coating was Ni-14Cr-14Al-0.1Zr, based on the time to thermal barrier crack initiation, specific weight change and post-test metallography. Of the eight bond coats evaluated on Mar M-509, a cobalt-base alloy, Ni-31Cr-11Al-0.6Y, was the best bond coating based on the previous criteria. In cyclic oxidation tests at 1100° C (2012° F) 14 bond coats were examined. The best bond coats were either Ni-14Cr-14-Al-0.1Zr or Ni-14Cr-14Al-0.1Y or Ni-16Cr-13Al-0.4Y on B-1900 + Hf and Ni-31Cr-11Al-0.5Y on Mar M-509. The effects of chromium, aluminum and yttrium content on oxidation behavior of bond coats are summarized, respectively, in figures 23, 24, and 25. If oxidation of bond coats is a major factor in degradation and failure of a thermal barrier coating system (leading to massive spallation of the thermal barrier coating), a bond coat with a low oxidation rate is very desirable. If this argument is true, based on the results presented in figures 23, 24, and 25, where loss of weight is assumed to be an indication of subsequent undesirable spalling, high chromium, moderate aluminum, and low yttriumtype bond coats might be best (see ref. 15).

In addition to the effect observed for composition changes of the bond coatings, coating deposition parameters affect oxidation behavior of bond coats. Although the study of the effects of changes in the deposition parameters has not been completed, it was found that oxidation resistance of the bond coatswas significantly improved by increasing the bond coat thickness (4 to 6 mils), arc current (350 to 450 amps) and hydrogen concentration in the arc gas (0 to 3.5 v/o). The results for the oxidation behavior of the bond coat Ni-31Cr-11Al-0.6Y on Mar M-509 as summarized in figure 26 typify the effect of the above changes in bond coating deposition parameters. The rapid weight lost between 100 and 150 hours for the parameters 4 mils/350 amp is indicative of massive spalling, which is undesirable.

SUBTASK 2.3.3 - REACTION STUDIES

In support of the burner rig tests, studies were conducted to determine how calcium orthosilicate (actual composition was $1.8CaO-SiO_2$) and barium zirconate powders react with powders of the potential combustion product compounds of major fuel and air impurities and with bond coating elements. The powder reactions were monitored as a function of time by X-ray diffraction. These reactions were studied at 1100° and 1300° C (2012° and 2372° F) for up to 400 and 200 hours, respectively. The results of these tests are presented in reference 16 and are summarized in Tables X and XI.

These tables list all the chemical compounds used and the products of their reactions with calcium silicate and barium zirconate at 1100° and 1300° C. They also include columns marked with the letters "N" or "Y" indicating that essentially no reaction took place (N) or that, yes, there was a partial or complete reaction (Y). The entry "unknown phase" was used when some lines of an X-ray diffraction pattern could not be attributed to any compound listed in the Powder Diffraction File Search Manual (ref. 17). In general, the heat treatments at 1100° and 1300° C produced similar results. When reactions were observed, they were usually the same at both temperatures. If there was no reaction at 1100°, there was generally none at 1300° C. The results of these reaction studies are summarized as follows:

1. The impurities that reacted with $2CaO-SiO_2$ are Na_2O, BaO, MgO, CoO, Al_2O_3, Cr_2O_3, P_2O_5 and V_2O_5.
2. The impurities that did not react with $2CaO-SiO_2$ are Na_2SO_4, K_2O, K_2SO_4, $BaSO_4$, NiO, ZnO and Fe_2O_3.
3. The impurities that reacted with $BaZrO_3$ are Al_2O_3, Fe_2O_3, Cr_2O_3, SiO_2, P_2O_5 and V_2O_5.
4. The impurities that did not react with $BaZrO_3$ are Na_2O, Na_2SO_4, K_2O, K_2SO_4, MgO, CaO, CoO and ZnO.

It is noteworthy that no monovalent or divalent oxides and sulfates reacted with barium zirconate. Similarly, calcium orthosilicate was not affected by sulfates, however, it was attacked by sodium, barium and cobalt oxides. Vanadium and phosphorous are impurities generally contained in industrial fuels and their pentoxides reacted readily with both barium zirconate and calcium orthosilicate.

TASK 3.0 - TECHNOLOGY EVALUATION STUDIES

SUBTASK 3.1 - THERMAL-BARRIER-COATING

LIQUID COOLING STUDY

This study was completed in FY 1978 and the results are presented in reference 18.

SUBTASK 3.2 - THERMAL BARRIER COATING-LOW CRITICAL ALLOY STUDY

The purpose of this study was to identify and quantify the potential cost savings that could result if the use of thermal barrier coatings on gas turbine hot section components permitted the decreased use of strategic alloys in these components. Thermal barrier coatings (TBC) could offer the potential for decreased use of strategic materials in utility gas turbines hot section alloys. By providing insulating protection between the corro-

sive hot gases and the metallic load-carrying members, the use of TBC's allow the metal substrate temperatures to be reduced. At the lower substrate temperatures, corrosion problems are reduced while material strength increases. Thus, some tradeoff may be made between turbine materials used in conjunction with thermal barrier coatings.

Some of the costs associated with the use of thermal barrier coatings on industrial gas turbine engines were studied (ref. 19). One of the cases studied compared the operating and maintenance costs of a current production turbine without a thermal barrier coating with the same turbine with thermal barrier coatings on blades, vanes, combustor liners and transition ducts. Turbine inlet temperatures and metal temperatures were the same for each machine and the cooling air flow rate was reduced to improve performance. It was assumed for this case that the thermal barrier coatings would have adequate durability to survive and protect the associated components for 2 years. For a peaking application (capacity factor 0.12) this would require at least 2100 hours of TBC life, and for a base load application (capacity factor of 0.65), a TBC life of about 12,000 hours would be required. With the 2-year life assumption, TBC component removal, inspection, stripping and reapplication would be conducted during a routine biennial turbine inspection in which the turbine casing would be opened. Thermal barrier coating stripping and recoating were estimated (by NASA) to be (mid-1975 $):

Combustor liner	$100 each
Transition piece	$200 each
Stationary vanes	$150/airfoil
Rotating blades	$150/airfoil

Based on these assumptions, the increased operating and maintenance costs associated with applying and maintaining thermal barrier coatings on these components amounts to 0.391 mills/kW-hr for the peaking application, and 0.048 mills/kW-hr for the baseload application. These costs represent approximately 25 to 50 percent of the cost of replacing turbine airfoils biennially.

As a result of certain "geo-political" considerations, the cost of various "critical" materials has risen dramatically in the recent past. Figure 27 illustrates te price of cobalt, chromium and tantalum over this time period. The price of other alloy materials may also be controlled by "geopolitical" considerations, rather than strictly economic considerations. It is estimated that this dramatic increase in cost of cobalt shown would increase the cost of a hypothetical 100 MW gas turbine engine by about $450,000 (an increase of about 3 percent in the capital cost of the system). The cost of applying TBC to the cooled airfoils and combustor hardware would be somewhat less than this initially (about $150,000 - 1979 $), but periodic stripping and reapplication would be required, as discussed above. Over the lifetime of the turbine, total costs would probably be about the same for either option. Summarizing the comparison of costs, there appears to be no large cost advantage for either option:

1. Utilizing conventional superalloys that are becoming more expensive as a result of "geopolitical" considerations.
2. Substituting alloys with lower contents of critical materials and protecting the hot section parts with thermal barrier coatings. However, it may be advantageous to the nation to achieve invulner-

ability to the supply of critical materials without a cost penalty.

In addition, qualification of a thermal barrier coating system in a production gas turbine system is expected to take a long time. Other factors, such as potential impact damage, inspection (NDE) and reapplication of ceramic coatings must be considered before TBC technology may be considered ready for the utility gas turbine market. Current DOE/NASA programs are addressing these considerations as well as TBC endurance.

SUBTASK 3.3 - FUEL/STACK/TEMPERATURE/PERFORMANCE STUDY

The effect on combined cycle performance of constraining the stack gas temperatures to levels high enough to avoid acid corrosion when burning high sulfur content fuels was studied; results are presented in reference 20 and summarized herein. The use of fuels containing sulfur requires that the cold-end heat exchanger surface and exhaust stack gas temperatures be kept above the sulfuric acid condensation temperatures. A high sulfur content fuel means a high acid concentration which then requires a high stack inlet temperature. Raising the exhaust stack gas temperature, however, results in lower combined cycle efficiency compared to that achievable by a combined cycle burning a sulfur-free fuel. Dew points were estimated as a function of fuel sulfur content and gas turbine design parameters. An equation based on experimental data was used for these dew points calculations. The effect on combined cycle efficiency was determined for air-cooled and water-cooled gas turbine/combined cycles. Combined cycle performance calculations were done first assuming a sulfur-free fuel, and then for a fuel with 0.8 percent sulfur content by weight. This is the maximum sulfur content for a liquid fuel that can be used without sulfur dioxide emission control devices and still meet environmental regulations.

The maximum differences found between the combined cycle performance using sulfur-free fuel and using the 0.8 percent sulfur fuel, was less than 1 percentage point in efficiency.

The combined cycle performance gains obtained by using thermal barrier coatings (TBC's) in gas turbine blades was previously investigated in reference 18. The performance calculations in reference 18, however, did not take into account the use of high sulfur fuel oils and the corresponding efficiency losses as mentioned above. When included in the analysis, the combined cycle efficiency gain of using TBC with a high sulfur fuel compared to a sulfur-free fuel fired combined cycle without TBC is 0.6 to 1.0 percentage points for the air-cooled gas turbine/combined cycles and 1.6 to 1.8 percentage points for the water-cooled gas turbine/combined cycles. Therefore, TBC's have the potential of allowing the use of the dirtier, less expensive, high sulfur fuels in gas turbines with an increase in efficiency. Without a TBC, the use of a dirtier, less processed fuel would require a reduction in gas turbine inlet temperature and, hence, a reduction in efficiency.

TASK 4.0 - CATALYTIC COMBUSTION STUDIES

Catalytic combustion has been demonstrated with low-nitrogen distillate fuels to achieve very low NO_x emissions along with high combustion efficiency. The purpose of this task is to demonstrate catalytic combustion with alternative fuels and to identify problem areas associated with the catalytic combustion of these fuels.

SUBTASK 4.1 - FIVE ATMOSPHERE ENDURANCE TESTS

The purpose of this subtask was to experimentally determine the durability of a catalyst burning No. 2 distillate oil for 1000 hours at five atmospheres pressure. The testing was conducted under contract at Englehard Industries, Inc. (NASA Contract No. NAS3-19416), and the results are presented in reference 21. Prior to the contract, the catalyst had been tested for 1000 hours at one atmosphere pressure and little degradation of performance was observed. These tests were conducted at simulated gas turbine steady-state operating conditions, using an air pre-heat temperature of 640 K (693° F), an inlet reference velocity of 14 meters per second, and an adiabotic flame temperature of the fuel/air mixture of 1533 K (2300° F).

The performance of the catalyst core was determined by monitoring emission throughout the test, periodically examining CO activity, and, at the beginning and end of the test, evaluating the performance of the catalyst over a wide parametric range of test conditions. Initial and final emissions results are summarized below:

	Initial after 63 hours	After 1014 hours	After 1062 hours
Unburned Hydrocarbons (ppm)	0	146	0
Carbon Monoxide (ppm)	30	2420	35
Nitrogen Oxides (ppm)	5.7	5.6	4.3

After the 1014 hours of testing, an unplanned 48-hour, 673 K (752° F) air soak was conducted while analytical system repairs were made. Apparently as a result of this air soak, the catalyst deactivation, which occurred gradually during the life test was reversed. As a result, the final performance tests showed only a slight degradation in catalyst performance.

SUBTASK 4.2 - PREVAPORIZED FUEL TESTS

An in-house investigation of catalytic combustion using heavy fuels was initiated in FY 1979. The study was intended to include two complementary efforts: (1) a demonstration of catalytic combustion with partially prevaporized residual fuels; and, (2) a demonstration of catalytic combustion with partially prevaporized coal-derived fuels.

The in-house effort was further subdivided into three ares: (1) tests of fuel injection systems, (2) evaluation of catalysts; and, (3) determination of fuel properties for the fuels being tested. Tests (1) and (2) were made in the flame-tube test rig illustrated in figure 28. Tests of fuel-injection systems were made using a hydrogen-fueled after burner in place of the catalytic reactor. Two types of fuel injectors were considered: a multiple-tube array which was previously used with success in distillate-fuel catalytic combustion studies (fig. 29), and a single-point Sonicore nozzle (fig. 30) injecting into a reduced area portion of the test duct. For inlet air temperatures in the range of 600° to 1200° F, fuel injectors plugged rapidly with the Bunker C fuel used if the entering fuel line was exposed to the inlet air stream. This problem was alleviated by cooling

the fuel lines to the injector. A second problem observed was the ignition of the fuel in the premixing portion of the duct. It has not yet been established if this upstream burning was due to autoignition of fuel droplets or to surface ignition of the fuel on the duct walls (which were observed to be coated with residue following each test). A multiple array of air-assist injectors has been designed which should provide much finer atomization than either of the injector types previously tested. This injector will be tested in FY 1980 to determine if improved atomization will overcome the upstream burning problem.

The duration of catalyst testing with Bunker C fuel was severely limited by the upstream burning problem. As a result, little parametric data was obtained. However, some conclusions can be drawn: With an inlet air temperature of 600° F, catalyst which became active with distillate fuels are inactive if Bunker C is introduced directly into a cold catalyst. With this same inlet temperature, however, oxidation of the Bunker C can be made to occur if the catalyst is first heated to operating temperature by using a distillate fuel before turning on the Bunker C flow. With inlet air temperatures above 800° F, Bunker C can be introduced to the cold catalyst without the use of a starting fuel. When the catalytic reactor was examined following these tests, residue was found on the upstream face; thus, it may be advisable to use an uncoated monolith for the first section of catalytic reactor for residual fuel use.

Tests of the properties of Bunker C included a standard atmospheric distillation and a simple surface ignition test. No distillate was obtained below 700° F (see fig. 31), and over 80 percent of the initial volume distilled off by the time a temperature of 900° F was obtained. Some of the remaining volume was a solid which was left on the bottom of the flask. During the surface-ignition tests, no flame resulted from dropping Bunker C onto a surface wth temperatures below 750° F. Higher surface temperatures did produce ignition of the fuel.

These tests show that it is virtually impossible to achieve complete vaporization of the residual fuels tested and that premixing of the fuel with hot air (greater than 750° F) will probably lead to burning in the premixing duct. A final decision on the advisability of operating in a premixed mode with residual fuels will depend on the results of the air-assist multiple-array fuel injector tests in FY 1980.

SUBTASK 4.3 - LIQUID SPRAY COMBUSTOR TESTS

The complementary effort to the in-house tests involves the demonstration of catalytic combustion with an incompletely vaporized residual fuel. Fuel-air mixtures with small (30 microns diameter) and large (70 to 120 microns) fueldroplets and less than 50 percent vaporization will be tested. During FY 1979, two contractors were selected: United Technologies and General Electric. The subcontractors responsible for catalytic reactor designs are Acurex and Engelhard, respectively. The UTRC contract was signed in July; rig design was initiated and testing continues. A multiple conical tube fuel injector has been used. The GE contract was signed early in FY 1980. A single-point air-assist nozzle will be tested. Testing in both contracts will be completed during FY 1981.

SUMMARY OF RESULTS

This 40-month project includes critical-research and advanced-technology efforts in combustion, materials, and systems studies. This report summarizes the technical progress made during FY 1979 to use coal-derived fuels in utility/industrial gas turbines. Earlier reports also summarized the project status at the end of FY 1978 and in mid-FT 1979, respectively (refs. 22 and 23). Significant progress has been made toward achieving the technical objectives of this work; this progress is summarized as follows:

1. A literature survey of properties of coal-derived fuels (literature through December 1977) was completed and published. A report summarizing subsequent literature is currently being prepared.
2. A combustor emission model has been assembled and compared with experimental data. Reasonable agreement was found. Rich/quick quench/lean combustion was modelled using a chemical kinetics model consisting of a two-stage, adiabatic, perfectly-stirred reactor.
3. Fundamental rich-lean combustion tests were conducted with varying hydrogen: carbon ratios, varying amounts of fuel bound nitrogen, and also with actual coal-derived fuels (SRC). Optimum primary equivalence ratio (for minimum NO_x) ranged from 1.4 to 1.7, while the optimum secondary equivalence ratio was about 0.5.
4. Doped-fuel materials corrosion tests were completed to study the corrosion effects of various contaminants (at various concentrations and temperature levels), and to determine the interrelationships of time, temperature, and contaminant on hot corrosion. This corrosion data was incorporated into a hot corrosion prediction model for the alloys and contaminants studied.
5. Potential fuel additives were also studied as a means of combating hot corrosion. Barium and strontium were found to be effective; intermittant application of the inhibitor was found to provide hot corrosion protection while reducing deposition.
6. Hot-corrosion tests of an SRC-II naphtha and a diesel fuel oil-micronized coal mixture yielded similar results. With both fuels, significant deposition occurred, but no erosion or hot corrosion was noted.
7. The LeRC Complex Chemical Equilibrium Calculation program was used to predict deposit compositions. Experiment verification tests were run and agreement was good between prediction and experiment.
8. Durability of duplex thermal barrier coating systems was found to be a strong inverse function of oxide thickness. Bond coating composition is also a strong factor in coating life. Several improved bond coatings were identified and evaluated.
9. Thermal barrier coating life criteria were studied; failures in various tests were correlated with thermodynamic dew points and melting points of the condensates and the temperature distributions within the coatings.
10. Several fundamental tests were run in support of the advanced thermal barrier coating efforts. Basic reaction studies contributed in-sight into the reactivity of thermal barriercoatings with various fuel impurities and bond coating constituents.
11. A preliminary study of the cost of applying thermal barrier coatings to gas turbine hot section components, compared to increased alloy costs (due to the spiraling costs of several "critical" ma-

terials), indicated no clear cost advantage with TBC's based on today's prices and assuming no restrictions on availability. As TBC's demonstrate acceptable durability, however, their use could permit reduced critical alloy use.

12. A study was made of the exhaust gas temperature of gas turbines required to avoid sulfuric acid condensation and corrosion in the cold-end heat exchangers when fuels of various sulfur levels are used. The results indicate that a combined cycle efficiency improvement of 0.6 to 1.0 percentage points can be realized when thermal barrier coatings are used to protect the hot section components (for an air-cooled turbine) even when the high exhaust temperatures are required.
13. A high-pressure (5-atmospheres) endurance (1000 hr) test of a catalytic combustor burning No. 2 fuel oil, was completed. Significant catalyst deactivity was noted during the 1000-hour test, but this activity was restored after an unplanned 673 K (752° F) air soak.
14. In-house tests were run with catalytic combustors burning heavy fuel oil and coal-derived fuels. With Bunker C residual fuel oil, combustion was limited by burning in the duct ahead of the catalytic combustor. Difficulties were also encountered in the uncooled fuels injector.

REFERENCE LIST

1. Reynolds, Thaine W.; Niedzwiecki, Richard W.; and Clark, John S.: Literature Survey of Properties of Synfuels Derived From Coal. DOE/NASA/2593-79/8, NASA TM-79243, 1980.
2. Bittker, David A.: An Analytical Study of NO_x and Carbon Monoxide Emissions in Hydrocarbon Combustion with Added Nitrogen - Preliminary Results. ASME Paper 80-GT-60, Mar. 1980; also DOE/NASA/2593-79/10, NASA TM-78296, 1979.
3. Schultz, Donald F. and Wolfbrandt, Gary: Flame Tube Parametric Studies for Control of Fuel Bound Nitrogen Using Rich-Lean Two-Stage Combustion. DOE/NASA/2593-80/15, NASA TM-81472, 1980.
4. Lowell, Carl E., Sidik, Steven M.; and Deadmore, Daniel R.: Effect of Sodium, Potassium, Magnesium, Calcium, and Chlorine on the High Temperature Corrosion of IN-100, U-700, IN-792, and Mar M-509. ASME Paper 80-GT-150, Mar. 1980; also DOE/NASA/2593-79/12, NASA TM-79309, 1980.
5. Deadmore, Daniel L.; and Lowell, Carl E.: Effects of Impurities in Coal-Derived Liquids on Accelerated Hot Corrosion of Superalloys. DOE/NASA/2593-79/13, NASA TM-81384, 1980.
6. Deadmore, Daniel L., and Lowell, Carl E.: Fouling and the Inhibition of Salt Corrosion. DOE/NASA/2593-80/14, NASA TM-81469, April 1980.
7. Gordon, Sanford; and McBride, Bonnie J.: Computer Program for Calculation of Complex Chemical Equilibrium Compositions, Rocket Performance, Incident and Reflected Shocks, and Chapman - Jouquet Detonations. NASA SP-273, 1971.
8. Deadmore, Daniel L.; and Lowell, Carl E.: Airfoil Cooling Hole Plugging by Combustion Gas Impurities of the Type Found in Coal-Derived Fuels. DOE/NASA/2593-79/1, NASA TM-79076, 1979.
9. Hodge, P. E.; et al: Thermal Barrier Coatings: Burner Rig Hot Corrosion Test Results. DOE/NASA/2593-78/3, NASA TM-79005, 1978.

10. Bratton, R. J.; Singhal, S. C.; and Hays, W.: Ceramic Rotor Blade Development, Part I - Ceramic Thermal Barrier Coatings. Semi-Annual Tech. Rep. -4, Westinghouse RaD Center, 1977.
11. Palko, J. E.; Luthra, K. L.; and McKee, D. W.: Evaluation of Performance of Thermal Barrier Coatings Under Simulated Industrial/Utility Gas Turbine Conditions. TID-29086, General Electric Co., 1978.
12. Miller, R. A.: Analysis of the Response of a Thermal Barrier Coating to Sodium and Vanadium-Doped Combustion Gases. DOE/NASA/2593-79/7, NASA TM-79205, June 1979.
13. Stecura, S.: Two-Layer Thermal Barrier Coating for High Temperature Components. Am. Ceramic Soc. Bulletin, Vol. 56, No. 12, 1977, pp 1082-1089.
14. Levine, S. R.: Adhesive/Cohesive Strength of a ZrO_2 12w/oY_2O_3/NiCrAlY Thermal Barrier Coating. NASA TM-73792, 1978.
15. Stecura, S.: The Effects of Yttrium, Aluminum and Chromium Concentrations on Bond Coatings on the Performance of Zirconia-Yttria Thermal Barriers, NASA TM-79206, 1979.
16. Zaplatynsky, Isidor: Reactions of Calcium Orthosilicate and Barium Zirconate with Oxides and Sulfates of Various Elements. DOE/NASA/2593-79/9, NASA TM-79272, 1979.
17. Powder Diffraction File Search Manual. Alphabetical Listing and Search Section of Frequently Encountered Phases (Inorganic), Publication SMA-26. Joint Committee on Powder Diffraction Standards, 1978.
18. Nainiger, Joseph J.: Effect of Thermal Barrier Coatings on the Performance of Steamand Water-Cooled Gas Turbine/Steam Turbine Combined Cycle Systems. DOE/NASA/2593-78/4, NASA TM-79057, Dec. 1978.
19. Amos, D. J.: Analytical Investigation of Thermal Barrier Coatings on Advanced Power Generation Gas Turbines. (EM-1636, Westinghouse Electric Corp.; NASA Contract NAS3-19407.) NASA CR-135146, March 1977.
20. Nainiger, Joseph J.: Effect of Combined Cycle Efficiency of Stack Gas Temperature Constraints to Avoid Acid Corrosion. DOE/NASA/2593-17, NASA TM-81531, July 1980.
21. Olson, B. A.; et al: Durability Testing at Five Atmospheres of Advanced Catalysts and Catalyst Supports for Gas Turbine Engine Combustors. DOE/NASA/9416-80/2, NASA CR-159839, April 1980.
22. Clark, John S.; et al: Gas Turbine Critical Research and Advanced Technology Support Project: FY 1978 Annual Report. DOE/NASA/2593-79/6, NASA TM-79139, 1979.
23. Clark, John S.: Status of the DOE/NASA Critical Gas Turbine RaT Project. ASME 80-GT-104, March 1980; also DOE/NASA/2593-79/11, NASA TM 79307, 1980.

TABLE I. - RESULTS OF HOT CORROSION MODEL REGRESSION ANALYSIS

	IN-100		U-700		IN-792		Mar M-509	
	ϕ_1	ϕ_2	ϕ_1	ϕ_2	ϕ_1	ϕ_2	ϕ_1	ϕ_2
Na	336.4	0.07666	105.2	0.06592	259.4	0.007793	2.667	0.2838
K	90.66	0.01373	13.10	0.1801	15.77	0.1606	8.384	0.1166
Mg	0.4661	2.039	0.7399	1.009	0.5489	2.598	2.773	0.02431
Cl	0.2312	0.5443	0.2430	0.3541	0.4104	0.5023	0.1856	0.1334
Ca	0.4345	6.000	0.6070	0.7410	0.1953	0.9624	0.4914	0.2500
β log t	0.9950		1.062		0.8218		0.6515	
β	-0.08192		-0.4103		0.3137		0.6720	
βT	-0.1234		0.1870		0.1227		0.05806	
βT^2	0.04424		-0.05006		-0.004882		0.02438	
βr_1	-0.05016		-0.09450		-0.05501		-0.02612	
βr_2	-0.02319		0.01082		-0.03358		-0.02606	
$\beta r_1 r_2$	0.01930		0.007929		-0.005913		0.001433	
SSQ TOT	44.54		44.06		25.01		13.23	
SSQ RES	7.19		7.53		4.23		3.86	
R^2	0.839		0.829		0.831		0.708	
n	203		200		205		203	
$\hat{\sigma}^2$	0.9387		0.0411		0.0225		0.0208	
$\hat{\sigma}$	0.197		0.203		0.150		0.144	
$10^{\pm 2\hat{\sigma}}$	(0.404, 2.47)		(0.393, 2.55)		(0.501, 1.99)		(0.515, 1.94)	

TABLE II. - METAL RECESSION AND DEPOSITION WITH ADDITIONS TO BARIUM INHIBITED HOT CORROSION

Additives, ppm	τ, μM				Deposit after washing, G			
	IN-100	U-792	IN-792	Mar M-509	IN-100	U-700	IN-792	Mar M-509
3-Na-3B-3Ca	410	74	61	70	[a]-0.99	0.86	0.88	0.93
3Mg	1680	62	100	80	[a]-7.19	.52	.61	.58
3Sr	23	47	10	61	1.00	.78	.92	.97
3Si	58	29	40	60	.04	.32	.29	.55
3Al	705	58	43	59	[a]-1.00	.32	.32	.32
3B	401	70	123	78	[a]-1.60	.38	.57	.64
-3Mn	1587	60	86	44	[a]-6.53	.32	.32	.40
-3Ni	819	52	83	42	[a]-5.00	.51	.63	.60
-3Zn	598	38	36	56	[a]-3.04	.35	.43	.42
-3P	1439	285	244	172	[a]-3.82	[a]-.55	.07	.04
-3Ph	1209	66	66	59	[a]-4.69	.57	.57	.57
3Na	2158	453	760	231	------	------	----	----
3Na + 3Ba	48	54	44	44	.03	.88	.81	.64

[a]Net loss, that is, corrosion excessive.

TABLE III. – PRECOATING EFFECTS ON DEPOSITION AND METAL LOSS

Inhibitor	Alloy	Deposition, 40 hours NoNa, G	Deposition, 40 hours 3Na, G	τ, no pre-coat, μm	τ, 40-hour precoat NoNa, μm	τ, 40-hour precoat 3Na, μm	τ, continuous inhibitor, μm
3Ba	IN-100	0.055	0.464	1530	750	1220	50
	U-700	.056	.358	180	20	----	50
	IN-792	.058	.303	490	120	170	40
	Mar M-509	.053	.345	190	40	110	40
3Sr	IN-100	.052	.449	1600	440	80	60
	U-700	.045	.465	----	---	----	60
	IN-792	.047	.443	610	100	60	30
	Mar M-509	.040	.448	330	110	70	70
3Ba + 3Sr	IN-100	.372	.818	1600	820	560	20
	U-700	.358	.830	----	---	----	--
	IN-792	.343	.819	430	30	60	10
	Mar M-509	.351	.866	290	40	30	60

TABLE IV. - TRACE METAL ANALYSES

(PPM) FOR SRC-II NAPHTHA

[Fuels used in hot corrosion tests.]

Element	Naphtha
Al	<0.01
Ca	<0.1
Cr	0.1
Cu	16 - 42
Fe	9
K	<0.25
Mg	<0.01
Mn	0.03 - 0.07
Na	<0.23
Ni	3 - 7
Pb	0.1 - 0.4
Si	0.1
Sr	0.1 - 0.2
Ti	0.2 - 0.3
Zn	7 - 16

TABLE V. - ELEMENTAL ANALYSIS OF MICRONIZED COAL IN DIESEL FUEL

Element	Spectographic analysis, ppm	Atomic absorption, ppm
Al	7 000 6 000	5300
Ca	1 400 1 500	750
Co	5 5	3.7
Cr	30 29	30
Cu	5 20	8.1
Fe	4 000 3 000	4500
Mg	210 250	230
Mn	50 30	26
Na	------ ------	100
Ni	40 30	27
Si	16 000 22 000	------
Ti	440 410	------
V	10 ------	<10
Zr	10 20	13.5
Total Cl:	638.0	294.0 ppm
Total S:	3716.0	2664.0 ppm

TABLE VI. - TRACE METAL ANALYSIS OF FUELS USED IN COMBUSTION ANALYSIS TESTS

[Combination of atomic absorption and light spectroscopy.]

Element	Naphtha	Light oil	Wash solvent
S, wt.%	0.61	0.40	0.33
Cl, wppm	49	<10	<10
Metals			
Ni	[a]4.8	[a]0.1	------
Cu	[a]28.9	.03	------
Fe	[a]8.8	158.	[a]35.7
Zn	[a]10.5	[a]2.5	[a].8
Pb	[a].3	<.07	------
Cr	[a].1	.04	.06
Al	<.01	-------	[a].9
Ca	<.01	[a].1	[a].6
Na	<.25	[a].6	[a].3
Si	.09	-------	[a].5
Mo	<<.01	-------	------
Ti	.03	-------	[a].8
Mn	.05	.4	.3
Mg	<<.01	.08	.07
K	<.25	[a].2	[a].4
V	<<.01	-------	------

[a]Metals considered in thermodynamic analysis.

TABLE VII. - COMPUTER PROGRAM PREDICTION OF CONDENSED PHASE COMPOSITION FROM SRC-II COMBUSTION

[1173 K]

Naphtha	Light oil	Wash solvent
CuO (S)[a]	Fe_2O_3 (S)[a]	Fe_2O_3 (S)[a]
Cu_2O (S)[b]	$CaSO_4$ (VW)	Al_2O_3 (M)
Fe_2O_3 (M)[b]	$NiFe_2O_4$ (VW)	SiO_2 (M)
$NiFe_2O_4$ (M)[a]	Na_2SO_4 (VVW)[c]	TiO_2 (M)
$CuFe_2O_4$ (W)[a,b]		CaO (M)[b]
$Cu_2Fe_2O_4$ (W)[a,b]		$CaSO_4$ (M)
$NiCr_2O_4$ (W)[a]		Na_2SO_4 (VVW)[c]
ZnO (W)[a,c]		
NiO (VW)[a,b]		
Cr_2O_3 (VW)[c]		

[a]Detected by XRD.
[b]Appear above 1173 K, but not stable at 1173 K.
[c]Appear at 1100 K.

TABLE VIII. - ANALYSIS OF DEPOSITS RESULTING FROM COMBUSTION OF SRC-II FUELS

[1173 K]

Technique	Naphtha	Light oil	Wash solvent
X-ray spectral diffraction	CuO (S) $(Cu,Ni,Zn)Fe_2O_4$ (S) $(Cu_{0,2}Ni_{0,8})O$ (M) ZnO (VW)	Fe_2O_3 (S)	Fe_2O_3 (S) Fe_3O_4 (S)
Emission spectroscopy	Cu (S) Fe (M) Ni (M) Zn (M) Cr (W)	Fe (S) Si (W) Al (W) Zn (W)	Fe (S) Si (M) Al (M) Cu (M) Ni (M) Zn (W)
X-ray spectral analysis	Cu (S) Fe (S) Ni (S) Zn (S)	Fe (S) Cu (T) K (T) Ca (T)	Fe (S) Si (M) Al (M) Cu (T) K (T) Ca (T) Ti (T)

TABLE IX. - RELATION BETWEEN CONDENSATE DEW AND MELTING POINTS AND $ZrO_2 \cdot 12Y_2O_3$/NiCrAlY PERFORMANCE

Dopant level (referred to fuel)	Predicted condensate	Dew point, T_{dp}, °C	Melting point, T_{mp}, °C	Condensate location	Cycles to coating failure
5 ppm Na	Na_2SO_4 (ℓ)	920	884	$T_s > T_{dp} > T_{mp} > T_{bc}$	92, out of hot zone
0.5 ppm Na	Na_2SO_4 (S)	845	884	$T_s > T_{mp} > T_{bc} > T_{dp}$	1300
2 ppm V	V_2O_5 (ℓ)	1210	670	$T_{dp} > T_s > T_{bc} > T_{mp}$	25, hot zone
0.2 ppm V	V_2O_5 (ℓ)	1125	670	$T_{dp} > T_s > T_{bc} > T_{mp}$	200, hot zone
5 ppm Na	V_2O_5 (ℓ)	1210	670	----------	
2 ppm V	$Na_2V_2O_6$ (ℓ)	~1155	627	$T_{dp} > T_s > T_{bc} > T_{mp}$	43, hot and cold zone
	Na_2SO_4 (ℓ)	~910	884	$T_s > T_{dp} > T_{mp} > T_{bc}$	
	V_2O_5 (S)	575	670	----------	

Mach 0.3 burner rig, fuel/air ratio 0.042; specimen temperatures: 982° C surface, (T_{surf}), 852° C bond coat/ceramic interface (T_{bc}) in the hot zone; 890° C surface, 760° C bond coat/ceramic interface at tip and root of test specimen.

TABLE X. - SUMMARY OF REACTIONS BETWEEN CALCIUM ORTHOSILICATE AND OXIDES AND SULFATES OF VARIOUS ELEMENTS

[Y - REACTION WAS DETECTED; N - NO REACTION WAS OBSERVED]

Temperature	1100° C				1300° C			
Time	200 hr		400 hr		100 hr		200 hr	
Na_2O	$2CaO \cdot SiO_2$ $Na_2O \cdot CaO \cdot SiO_2$	Y	$2CaO \cdot SiO_2$ $Na_2O \cdot CaO \cdot SiO_2$	Y	$2CaO \cdot SiO_2$ $Na_2O \cdot CaO \cdot SiO_2$	Y	$2CaO \cdot SiO_2$ Unknown phase $Na_2O \cdot CaO \cdot SiO_2$ (trace)	Y
Na_2SO_4	$2CaO \cdot SiO_2$ Unknown phase	N	$2CaO \cdot SiO_2$ Unknown phase	N	$2CaO \cdot SiO_2$ Unknown phase	N	$2CaO \cdot SiO_2$ Unknown phase	N
K_2O	$2CaO \cdot SiO_2$	N	$2CaO \cdot SiO_2$	N	$2CaO \cdot SiO_2$	N	$2CaO \cdot SiO_2$	N
K_2SO_4	$2CaO \cdot SiO_2$ K_2SO_4	N	$2CaO \cdot SiO_2$ K_2SO_4	N	$2CaO \cdot SiO_2$ K_2SO_4 Unknown phase	N	$2CaO \cdot SiO_2$ Unknown phase K_2SO_4 (trace)	N
BaO	$2(Ca_xBa_{1-x})SiO_4$ CaO?	Y	$2(Ca_xBa_{1-x})SiO_2$ CaO?	Y	$2(Ca_xBa_{1-x}) \cdot SiO_2$ CaO?	Y	$2(Ca_xBa_{1-x}) \cdot SiO_2$ CaO?	Y
$BaSO_4$	$2CaO \cdot SiO_2$ $BaSO_4$	N	$2CaO \cdot SiO_2$ $BaSO_4$	N	$2CaO \cdot SiO_2$ $BaSO_4$	N	$2CaO \cdot SiO_2$ $BaSO_4$	N
MgO	MgO $2CaO \cdot SiO_2$	Y	MgO $2CaO \cdot SiO_2$	Y	MgO Unknown phase	Y	MgO Unknown phase	Y
NiO	$2CaO \cdot SiO_2$ NiO	N	$2CaO \cdot SiO_2$ NiO	N	$2CaO \cdot SiO_2$ NiO	N	$2CaO \cdot SiO_2$ NiO	N
CoO	CoO $2CaO \cdot SiO_2$ Unknown phase (trace)	Y	CoO $2CaO \cdot SiO_2$ Unknown phase (trace)	Y	CoO Unknown phase $2CaO \cdot SiO_2$ (trace)	Y	CoO Unknown phase $2CaO \cdot SiO_2$ (trace)	Y
ZnO	$2CaO \cdot SiO_2$ ZnO	N	$2CaO \cdot SiO_2$ ZnO	N	$2CaO \cdot SiO_2$ ZnO	N	$2CaO \cdot SiO_2$ ZnO	N
Fe_2O_3	$2CaO \cdot SiO_2$ Fe_2O_3	N	$2CaO \cdot SiO_2$ Fe_2O_3	N	$2CaO \cdot SiO_2$ Fe_2O_3 Unknown phase	N	$2CaO \cdot SiO_2$ Fe_2O_3 Unknown phase	N
Al_2O_3	$3CaO \cdot Al_2O_3 \cdot SiO_2$ $2CaO \cdot SiO_2$	Y	$2CaO \cdot Al_2O_3 \cdot SiO_2$ $2CaO \cdot SiO_2$	Y	$2CaO \cdot Al_2O_3 \cdot SiO_2$ $2CaO \cdot SiO_2$	Y	$2CaO \cdot Al_2O_3 \cdot SiO_2$ $2CaO \cdot SiO_2$	Y
Cr_2O_3	$3CaO \cdot Cr_2O_3 \cdot SiO_2$ $2CaO \cdot SiO_2$	Y	$3CaO \cdot Cr_2O_3 \cdot SiO_2$ $2CaO \cdot SiO_2$	Y	$2CaO \cdot SiO_2$ Cr_2O_3	Y	$2CaO \cdot SiO_2$ Cr_2O_3	Y
P_2O_5	One or two unknown phases	Y	One or two unknown phases	Y	$3CaO \cdot P_2O_5$ Unknown phase SiO?	Y	$3CaO \cdot P_2O_5$ Unknown phase SiO?	Y
V_2O_5	Unknown phase some V_2O_5	Y	Unknown phase trace of V_2O_5	Y	Sample lost	Y	Sample lost	Y

TABLE XI. - SUMMARY OF REACTIONS BETWEEN BARIUM ZIRCONATE AND OXIDES AND SULFATE OF VARIOUS ELEMENTS

[Y- REACTION WAS DETECTED; N - NO REACTION WAS OBSERVED]

Temperature	1100° C				1300° C			
Time	200 hr		400 hr		100 hr		200 hr	
Na_2O	$BaZrO_3$ Unknown phase	N	$BaZrO_3$ Unknown phase	N	$BaZrO_3$ Unknown phase	N	$BaZrO_3$ Unknown phase	N
Na_2SO_4	$BaZrO_3$ Unknown phase	N	$BaZrO_3$ Unknown phase	N	$BaZrO_3$ Unknown phase	N	$BaZrO_3$ Unknown phase	N
K_2O	$BaZrO_3$	N	$BaZrO_3$	N	$BaZrO_3$	N	$BaZrO_3$	N
K_2SO_4	$BaZrO_3$ K_2SO_4 (trace)	N	$BaZrO_3$ K_2SO_4 (trace)	N	$BaZrO_3$ K_2SO_4 (trace)	N	$BaZrO_3$ K_2SO_4 (trace)	N
MgO	$BaZrO_3$ MgO	N	$BaZrO_3$ MgO	N	$BaZrO_3$ MgO	N	$BaZrO_3$ MgO	N
CaO	$BaZrO_3$ CaO	N	$BaZrO_3$ CaO	N	$BaZrO_3$ CaO	N	$BaZrO_3$ CaO	N
NiO	$BaZrO_3$ NiO	N	$BaZrO_3$ NiO	N	$BaZrO_3$ NiO	N	$BaZrO_3$ NiO	N
CoO	$BaZrO_3$ CoO	N	$BaZrO_3$ CoO	N	$BaZrO_3$ CoO	N	$BaZrO_3$ CoO	N
ZnO	$BaZrO_3$ ZnO	N	$BaZrO_3$ ZnO	N	$BaZrO_3$ ZnO	N	$BaZrO_3$ ZnO	N
Fe_2O_3	$BaZrO_3$ $BaO \cdot 6Fe_2O_3$ ZrO_2 (mon)	Y	$BaZrO_3$ $BaO \cdot 6Fe_2O_3$ ZrO_2 (mon)	Y	$BaZrO_3$ $BaO \cdot 6Fe_2O_3$ ZrO_2 (mon)	Y	$BaZrO_3$ $BaO \cdot 6Fe_2O_3$ ZrO_2 (mon)	Y
Al_2O_3	$BaZrO_3$ $BaO \cdot Al_2O_3$ ZrO_2 (mon)	Y	$BaZrO_3$ $BaO \cdot Al_2O_3$ ZrO_2 (mon)	Y	$BaZrO_3$ $BaO \cdot Al_2O_3$ ZrO_2 (mon)	Y	$BaZrO_3$ $BaO \cdot Al_2O_3$ ZrO_2 (mon)	Y
Cr_2O_3	$BaCrO_4$ ZrO_2 (mon) Cr_2O_3?	Y	$BaCrO_4$ ZrO_2 (mon) Cr_2O_3?	Y	$BaCrO_4$ ZrO_2 (mon) Cr_2O_3?	Y	$BaCrO_4$ ZrO_2 (mon) Cr_2O_3?	Y
SiO	$2BaO \cdot 2ZrO_3 \cdot 3SiO_2$ $BaZrO_3$ SiO_2 (trace)?	Y	$2BaO \cdot 2ZrO_3 \cdot 3SiO_2$ $BaZrO_3$ SiO_2 (trace)?	Y	$2BaO \cdot 2ZrO_3 \cdot 3SiO_2$ $BaZrO_3$	Y	$2BaO \cdot 2ZrO_3 \cdot 3SiO_2$ $BaZrO_3$	Y
P_2O_5	$BaO \cdot ZrO_2 \cdot P_2O_5$ Unknown phase	Y	$BaO \cdot ZrO_2 \cdot P_2O_5$ Unknown phase	Y	$BaO \cdot ZrO_2 \cdot P_2O_5$ Unknown phase	Y	$BaO \cdot ZrO_2 \cdot P_2O_5$ Unknown phase	Y
V_2O_5	$3BaO \cdot V_2O_5$ ZrO_2 (mon) Unknown phase	Y	$3BaO \cdot V_2O_5$ ZrO_2 (mon)O Unknown phase	Y	$3BaO \cdot V_2O_5$ ZrO_2 (mon) Unknown phase	Y	$3BaO \cdot V_2O_5$ ZrO_2 (mon) Unknown phase	Y

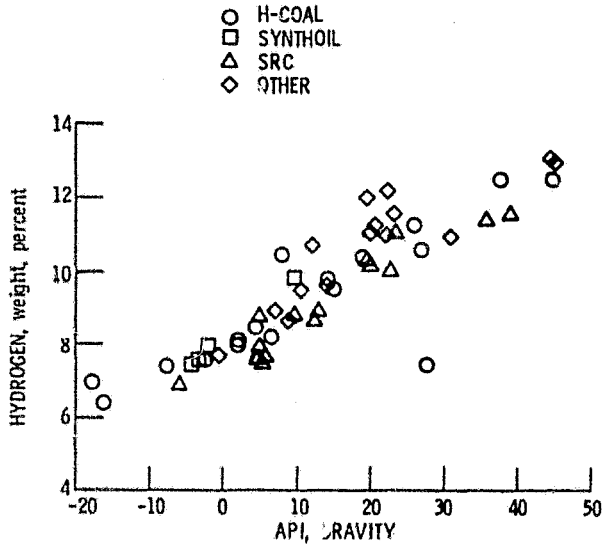

Figure 1. - Variation of hydrogen content of coal-derived fuels with API gravity.

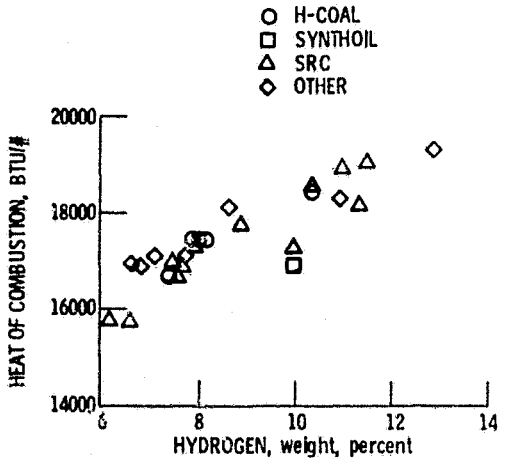

Figure 3. - Variation of heat-of-combustion of coal-derived fuels with hydrogen content.

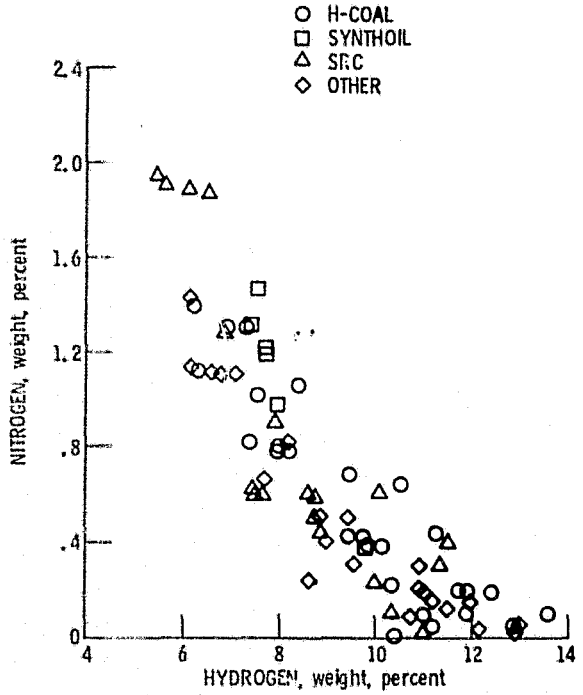

Figure 2. - Relation of fuel-bound nitrogen and hydrogen levels in coal-derived fuels.

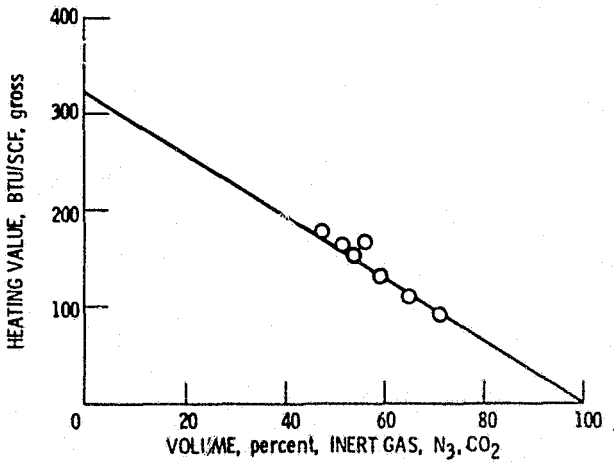

Figure 4. - Gross heating value of low-BTU gases as function of inert gas content.

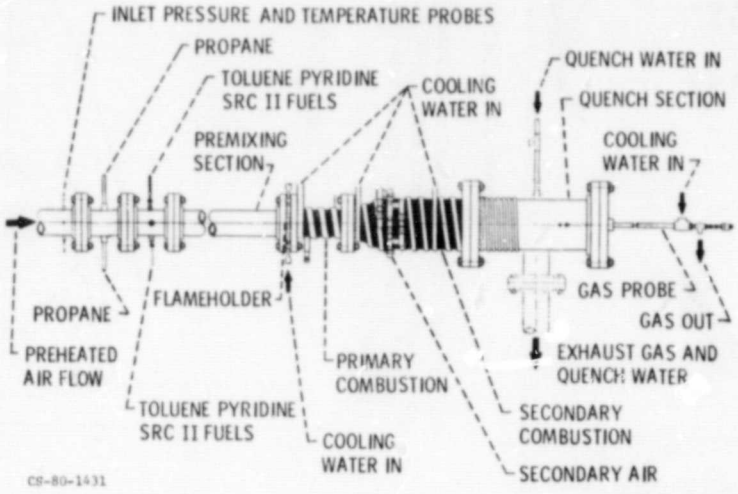

Figure 5. - Flame tube test rig.

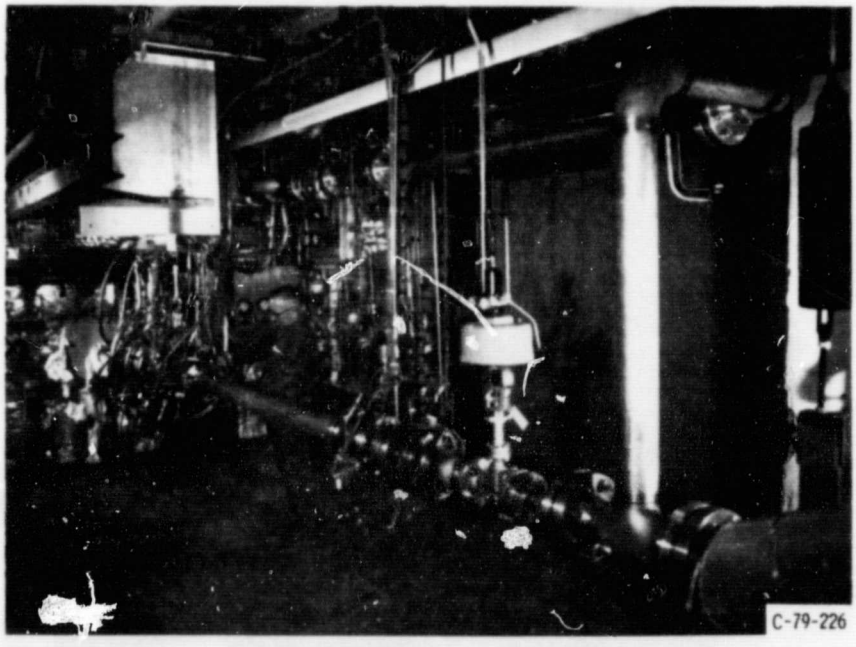

Figure 6. - Photograph of the test rig.

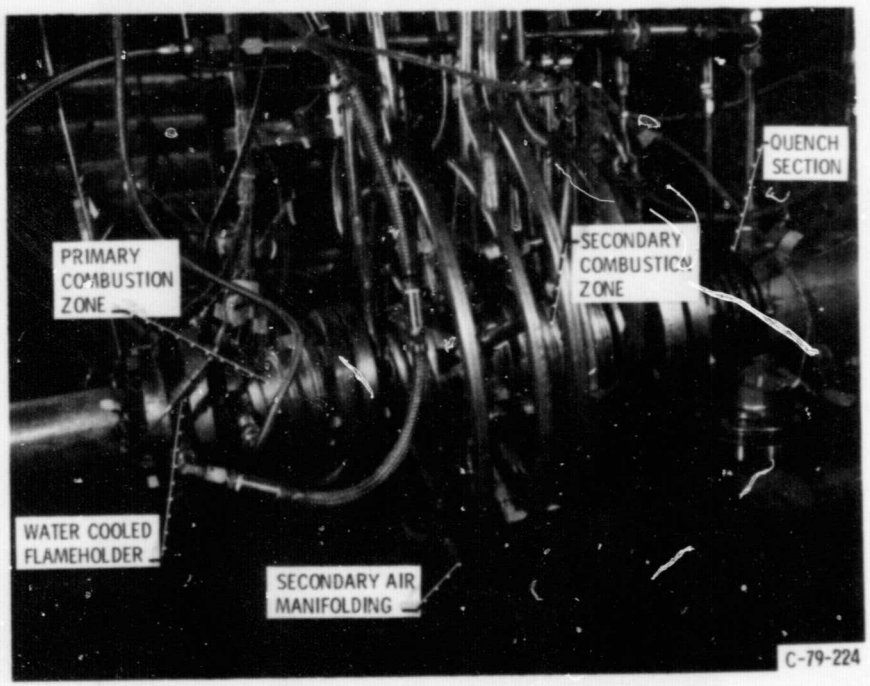

Figure 7. - Photograph of the combustion sections.

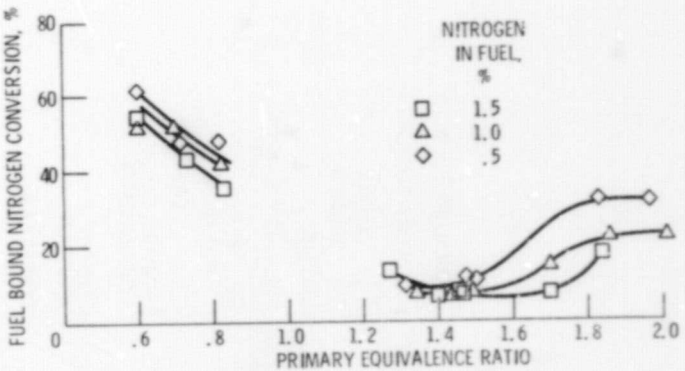

(a) Fuel bound nitrogen conversion versus primary equivalence ratio for a 9% hydrogen fuel blend. Inlet air at 672 K and 0.48 MPa; 6030 cm^3 primary volume; 2 msec secondary residence time ~0.5 secondary φ.

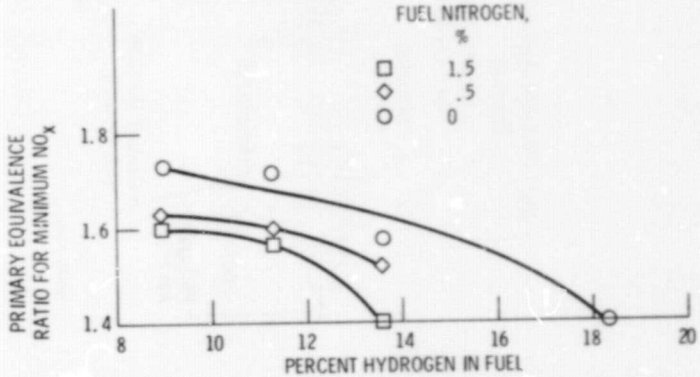

(b) Optimum primary equivalence ratio versus fuel hydrogen content. Inlet air at 672 K and 0.48 MPa; 6030 cm^3 primary volume 2 msec secondary residence time ~0.5 secondary φ.

Figure 8. - Test results.

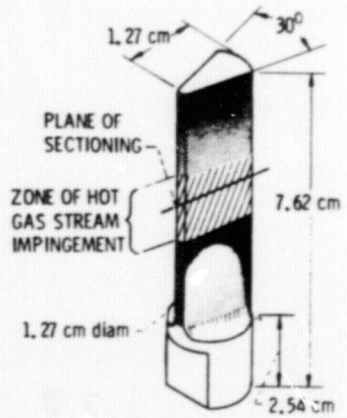

(a) TEST BAR.

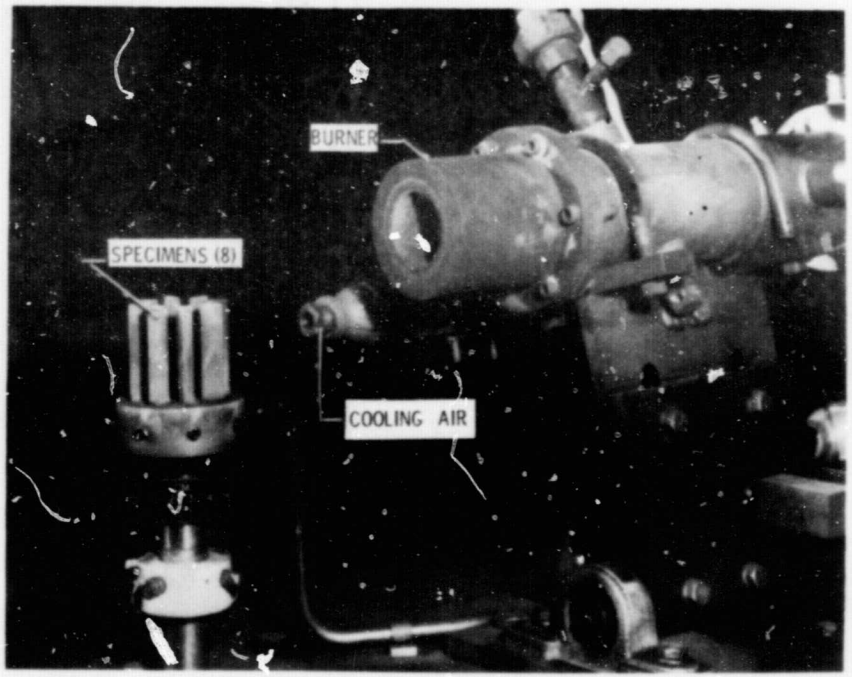

(b) BURNER RIG.

Figure 9. - Hot corrosion apparatus and test specimen.

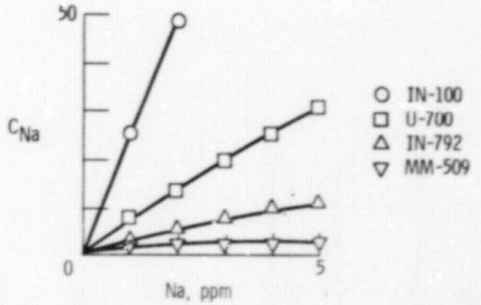

(a) SODIUM.

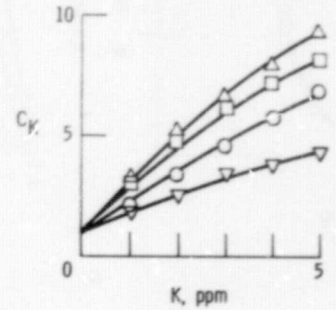

(b) POTASSIUM.

Figure 10. - Effect of concentration on C_i using pass 2 data.

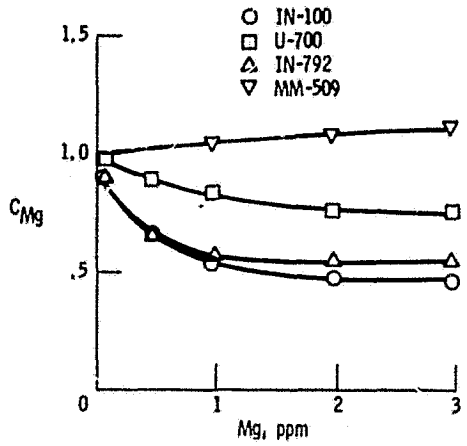

(c) MAGNESIUM.

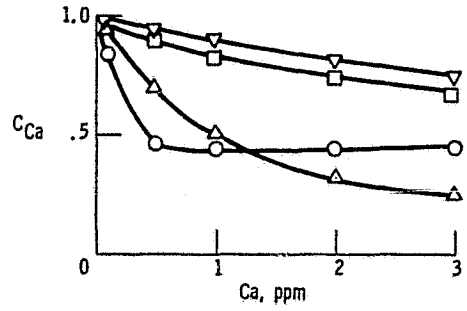

(d) CALCIUM.

Figure 10. - Continued.

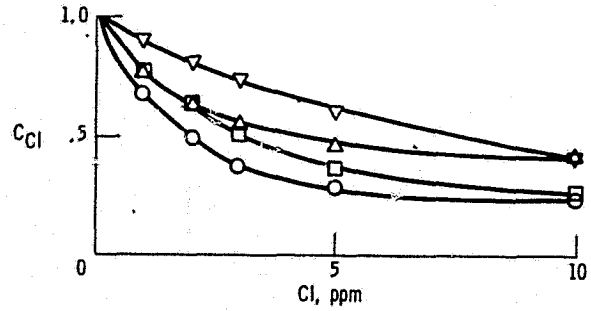

(e) CHLORINE.

Figure 10. - Concluded.

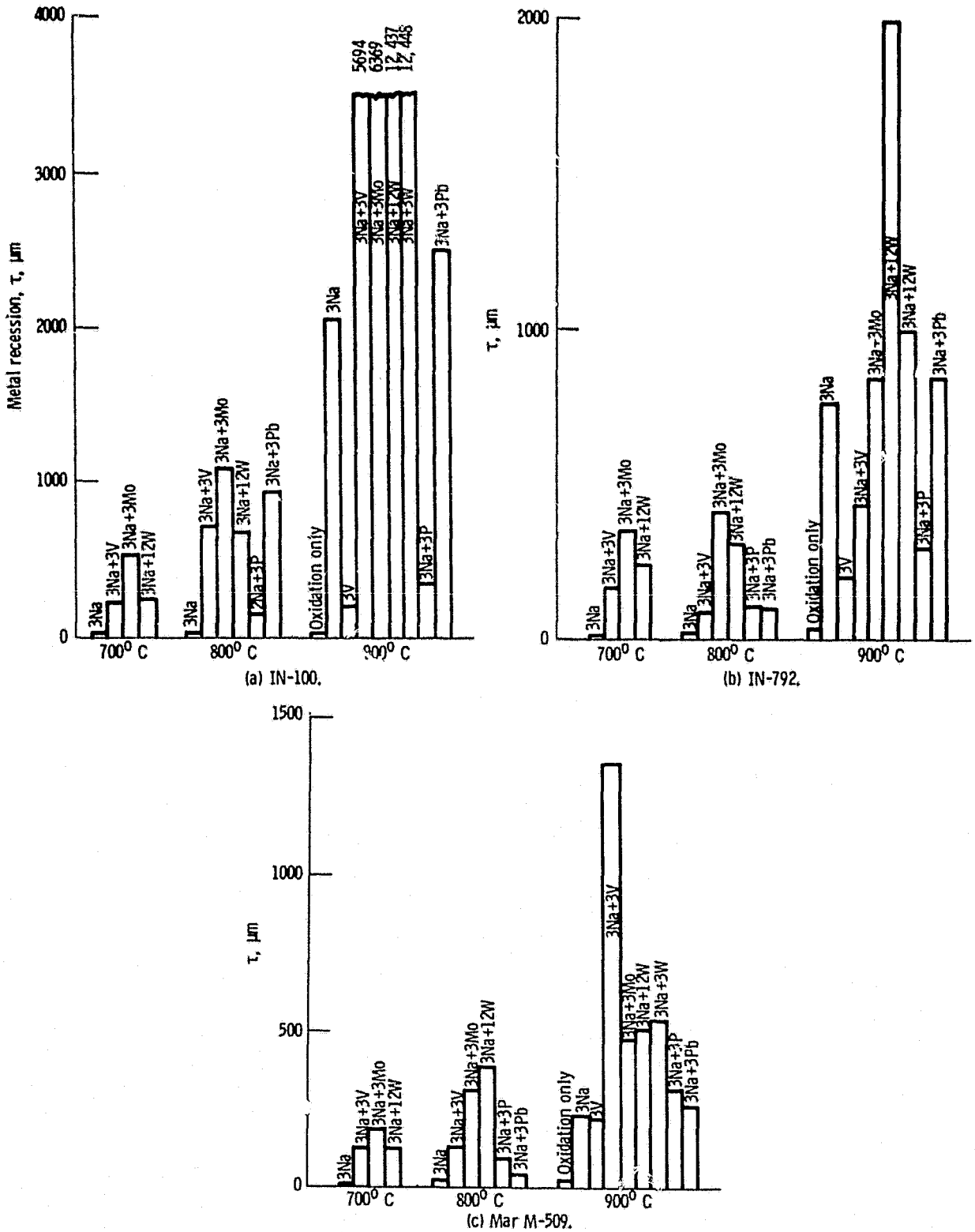

Figure 11. - Effect of potential coal-derived liquid fuel impurities on hot corrosion. One hundred cycles of 1 hour at temperature in a Mach 0.3 burner rig.

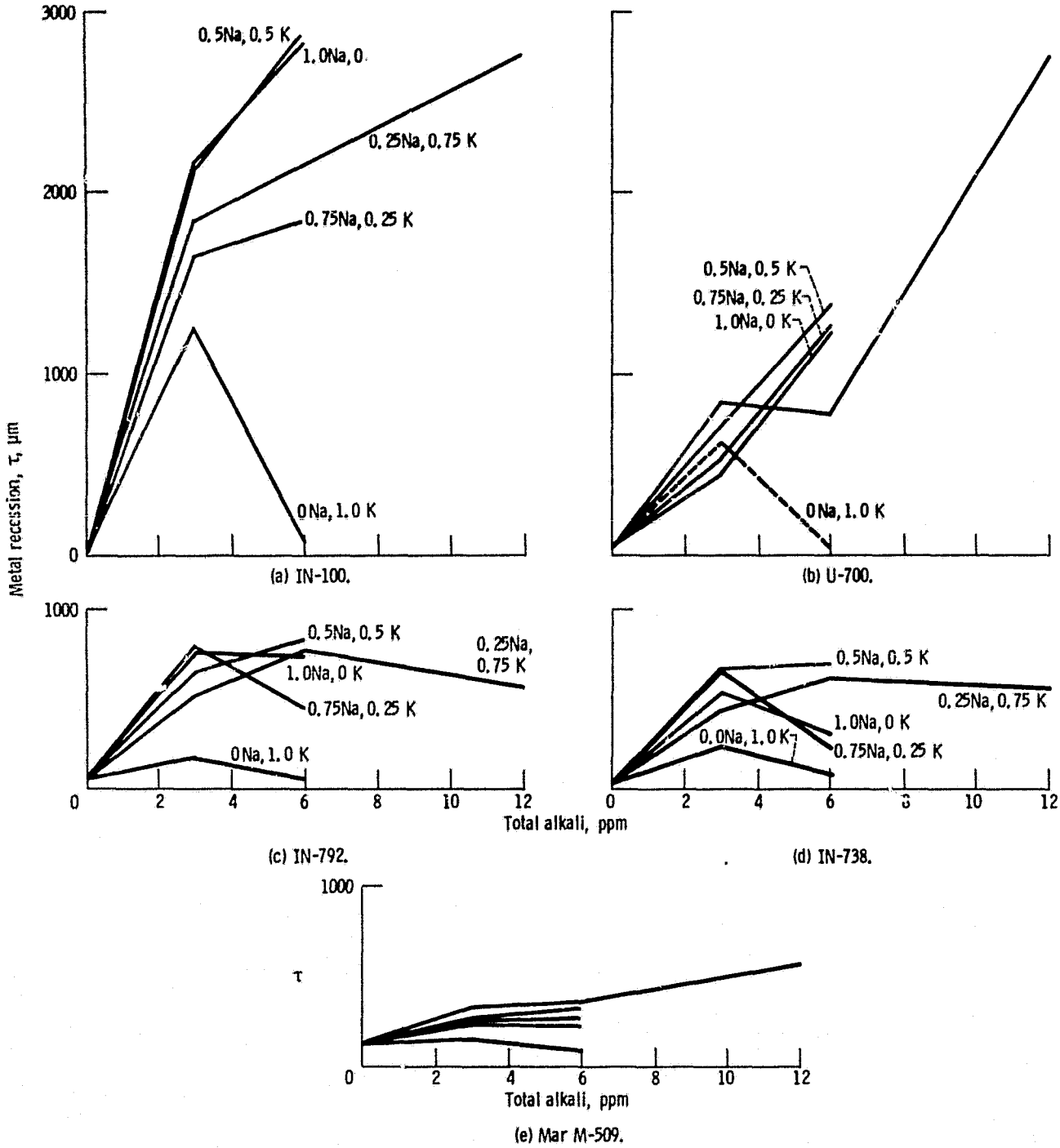

Figure 12. - Effect of total alkali on hot corrosion. One hundred cycles of 1 hour at 900° C in a Mach 0.3 burner rig.

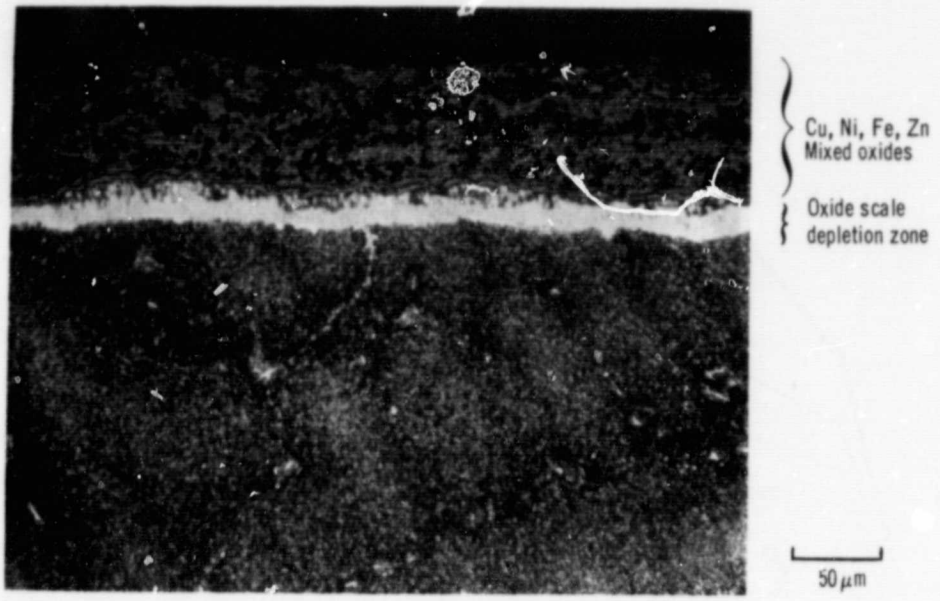

Figure 13. - The microstructure of U-700 after 192 hours at 900°C SRC II naptha.

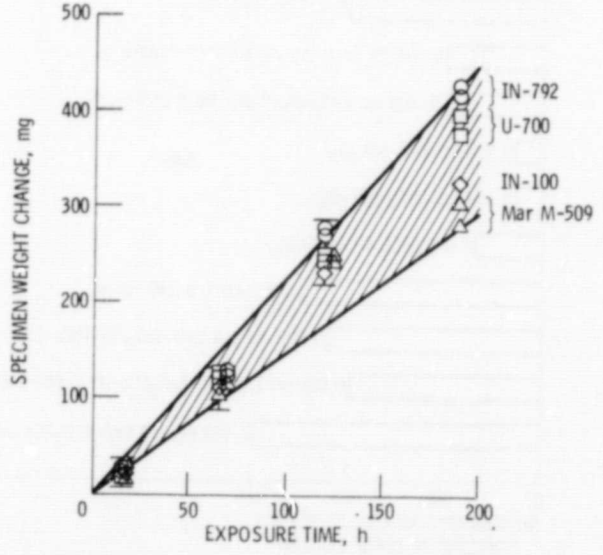

Figure 14. - Deposition rates for SRC-II naphtha tests.

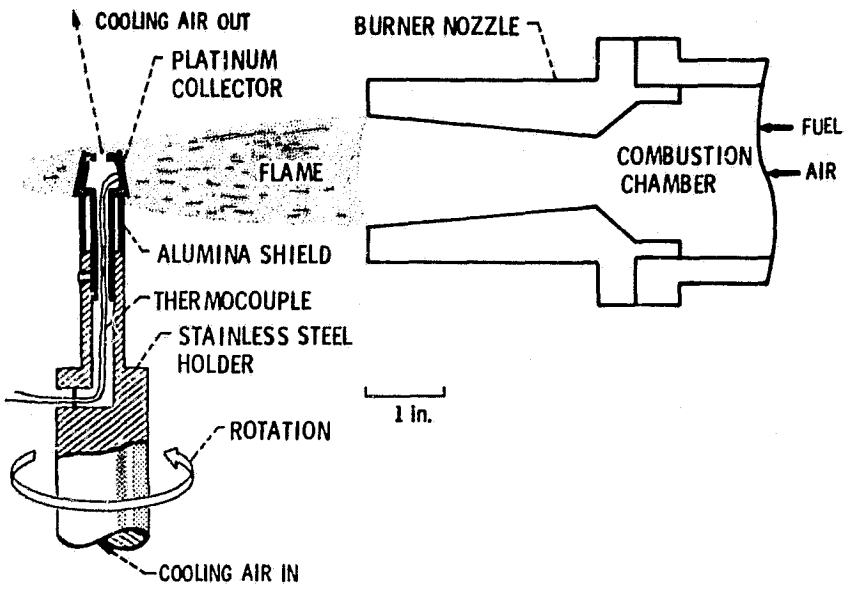

Figure 15. - Schematic cross-section of burner rig deposition apparatus.

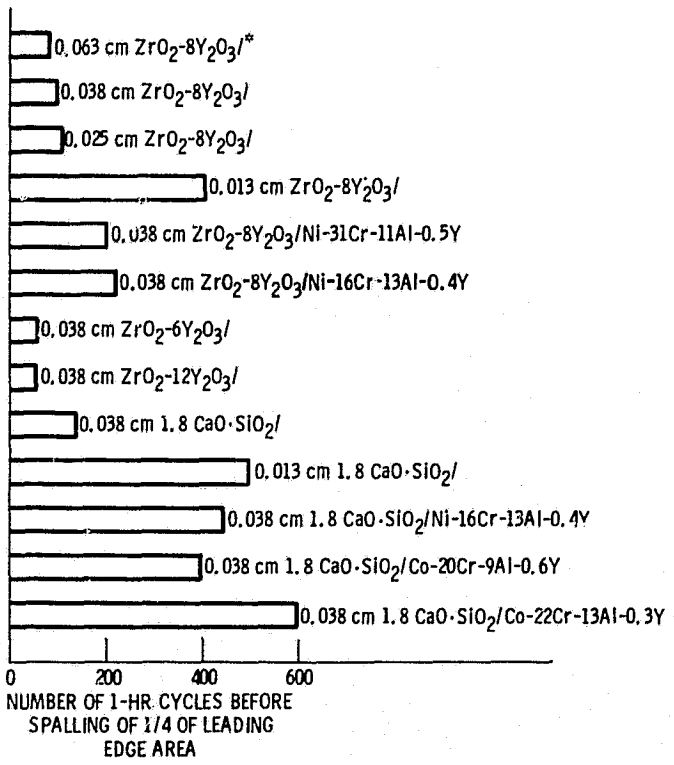

*BOND COATING IS 0.013 cm Ni-16Cr-6Al-0.3Y UNLESS OTHERWISE SPECIFIED.

Figure 16. - Mach 0.3 burner rig corrosion test: fuel impurity level, 5 ppm Na + 2 ppm V; fuel/air = 0.046; ceramic surface temperature, 982° C; substrate temperature, 843° C.

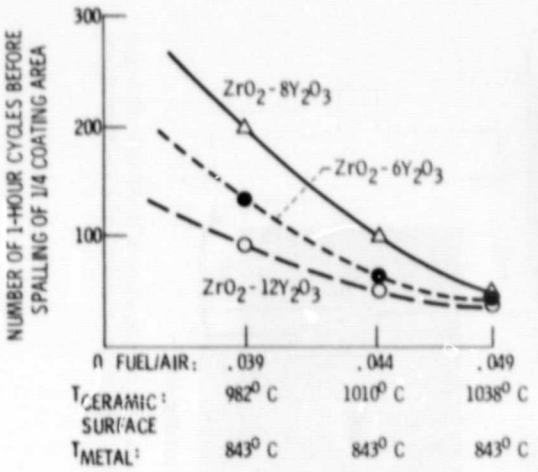

Figure 17. - Fuel-to-air mass ratio burner rig study. Fuel impurity level 5 ppm Na + 2 ppmV substrate: 1/2 in. O.D. Waspaloy; bond coat: Ni-16Cr-6Al-0.31Y.

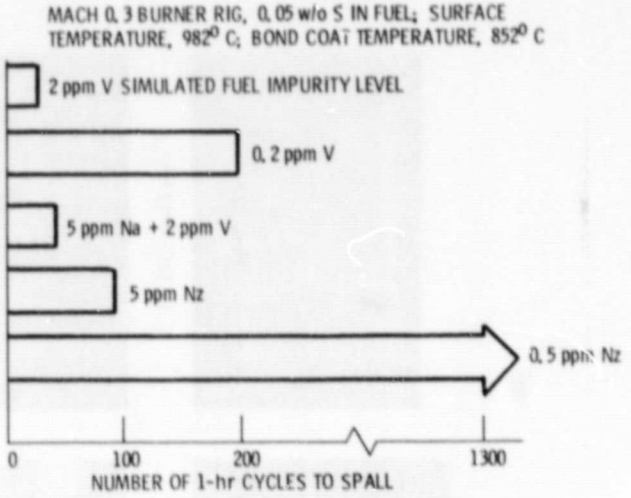

Figure 18. - Results of ZrO_2 - 12w/oY_2O_3 TBC fuel impruity sensitivity tests.

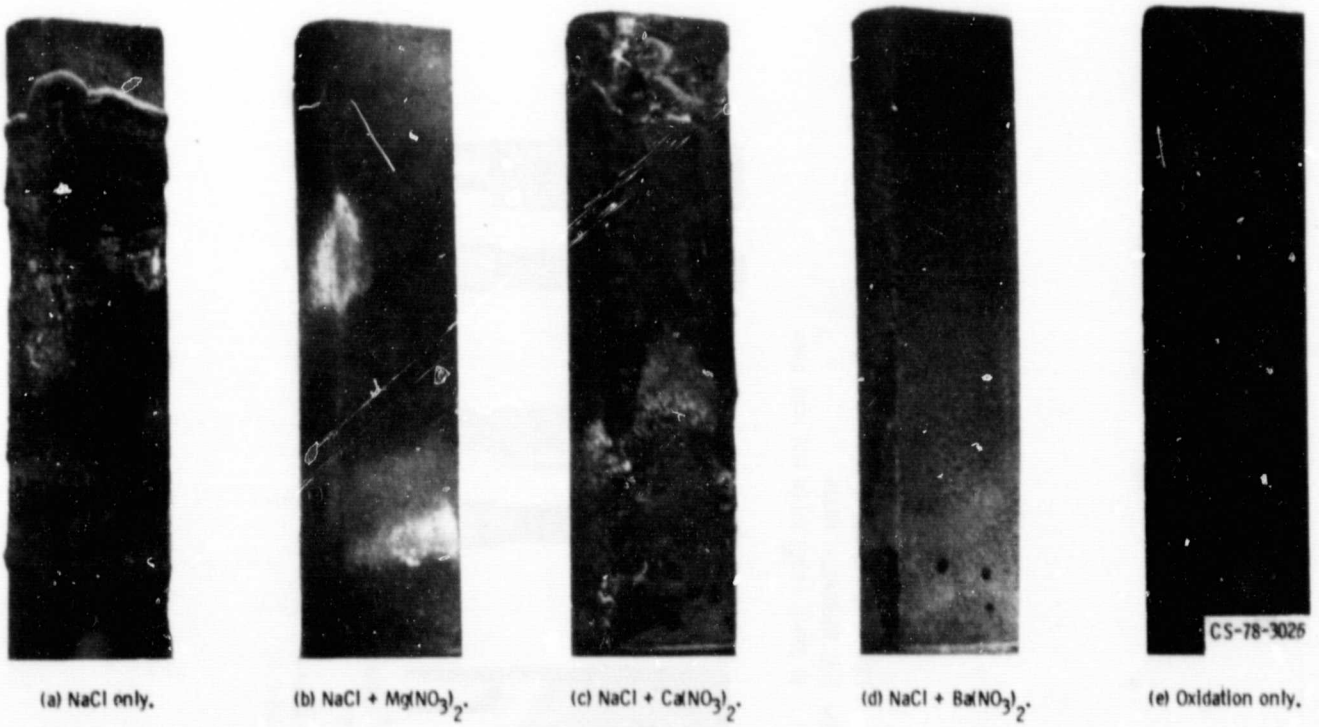

(a) NaCl only. (b) NaCl + $Mg(NO_3)_2$. (c) NaCl + $Ca(NO_3)_2$. (d) NaCl + $Ba(NO_3)_2$. (e) Oxidation only.

Figure 19. - Effect of alkaline earth additions on deposition on and corrosion of IN-792 after 100 1-hour cycles at 900° C (1652° F) and Mach 0.3. All additive concentrations are at 3 ppm of each metal.

MACH 0.3 BURNER RIG

TEMPS: 1370° C FLAME, 982° C CERAMIC SURFACE, 843° C METAL

DOPANTS: FUEL EQUIVALENT BASIS

TIMES: TO SPALL ABOUT 1/4 OF HOT ZONE AREA

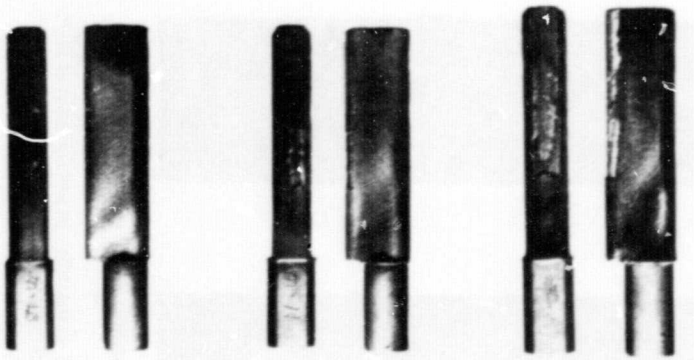

200 ONE-hr CYCLES
0.2 ppm V

25 ONE-hr CYCLES
2 ppm V

43 ONE-hr CYCLES
5 ppm Na + 2 ppm V

CS-79-2818

Figure 20 - Effect of vanadium and sodium plus vanadium on $ZrO_2 \cdot 12w/oY_2O_3$/ Ni-16Cr-6Al-0.6Y.

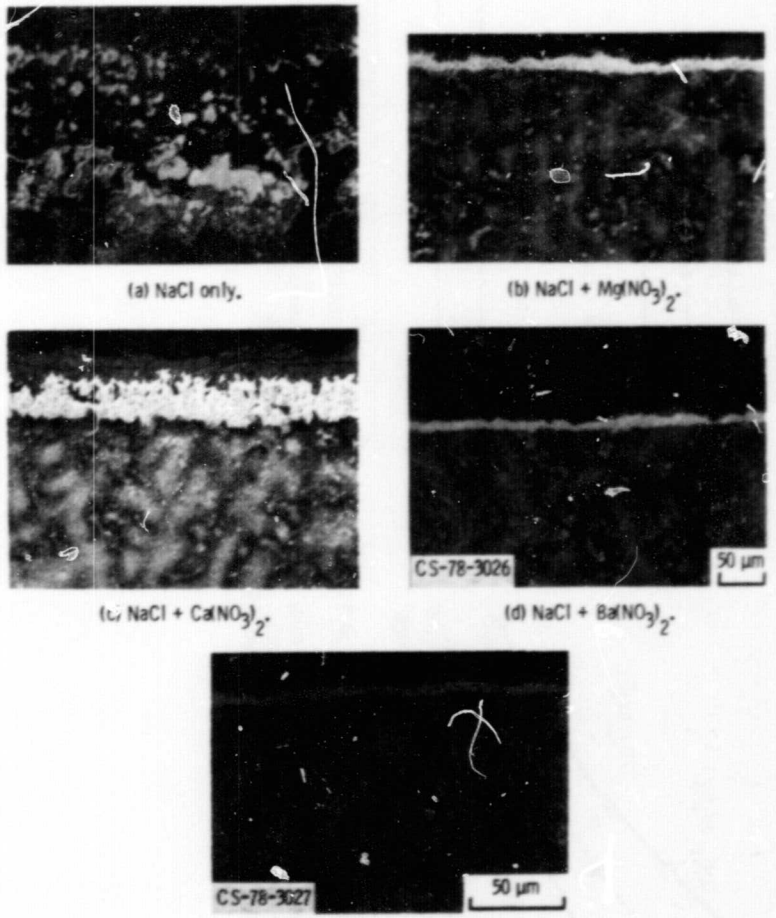

(a) NaCl only.

(b) NaCl + $Mg(NO_3)_2$.

(c) NaCl + $Ca(NO_3)_2$.

(d) NaCl + $Ba(NO_3)_2$.

(e) Oxidation only.

Figure 21. - Effect of alkaline earth additions on microstructure of IN-792 after 100 1-hour cycles at 900° C (1652° F) and Mach 0.3. All additive concentrations are at 3 ppm of each metal.

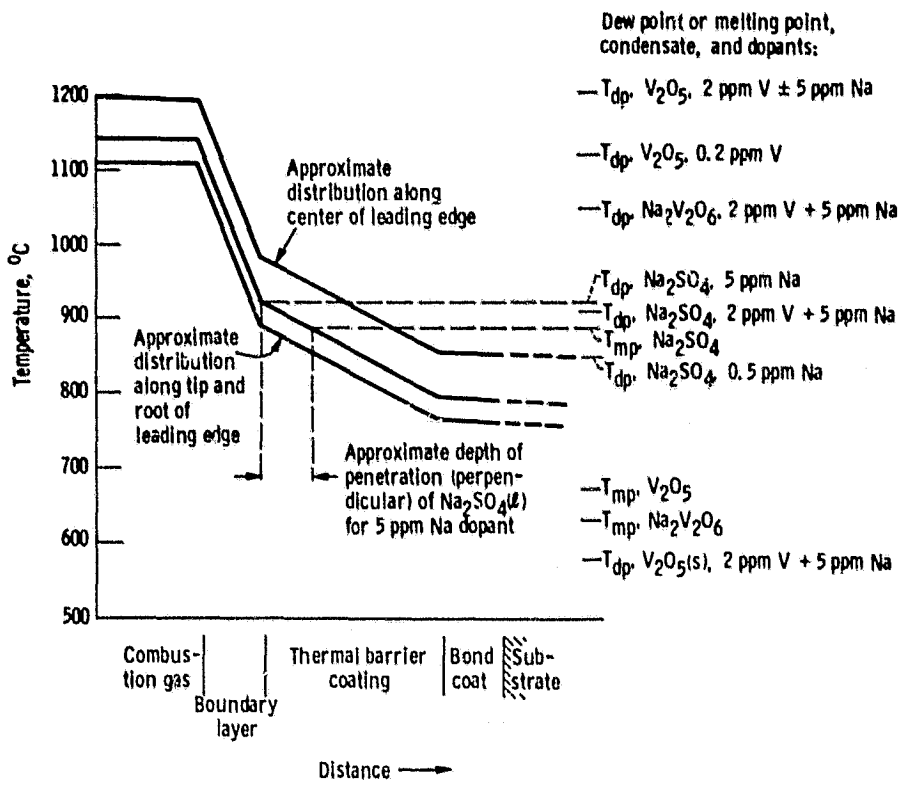

Figure 22. - Penetration of ZrO_2 . 12w/oY_2O_3 by Na_2SO_4 when 5 ppm of Na is present in the fuel.

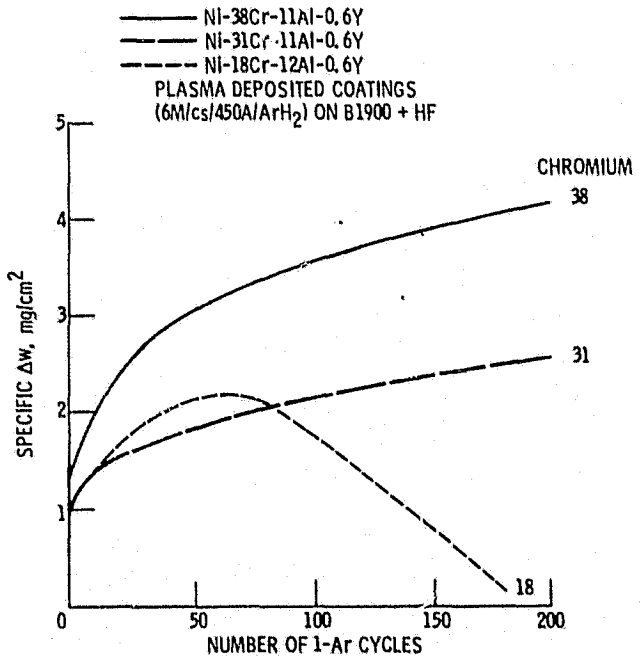

Figure 23. - Effect of chromium on NiCrAlY oxidation at 2012° F.

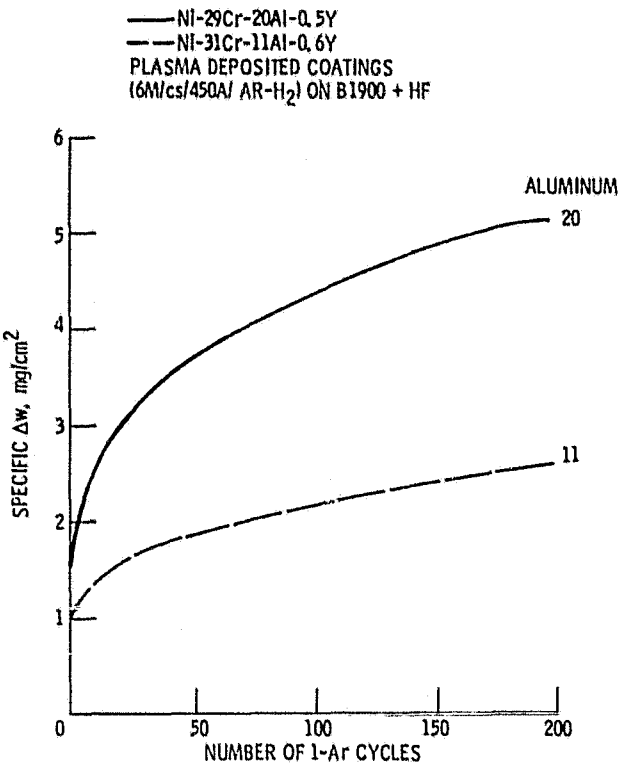

Figure 24. - Effect of aluminum on NiCrAlY oxidation at 2012^0 F.

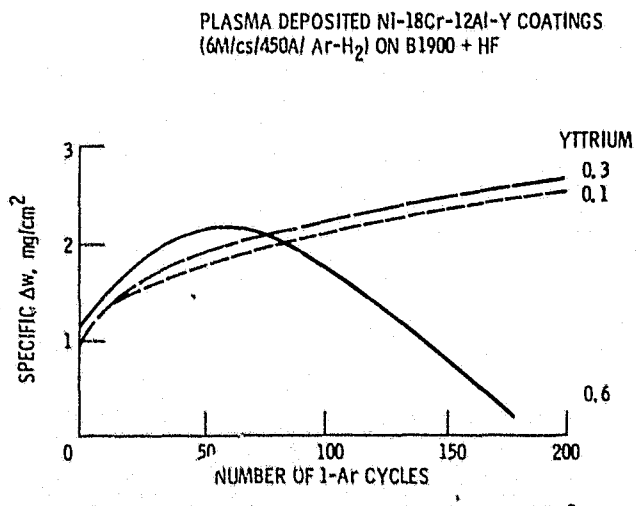

Figure 25. - Effect of yttrium on NiCrAlY oxidation at 2012^0 F.

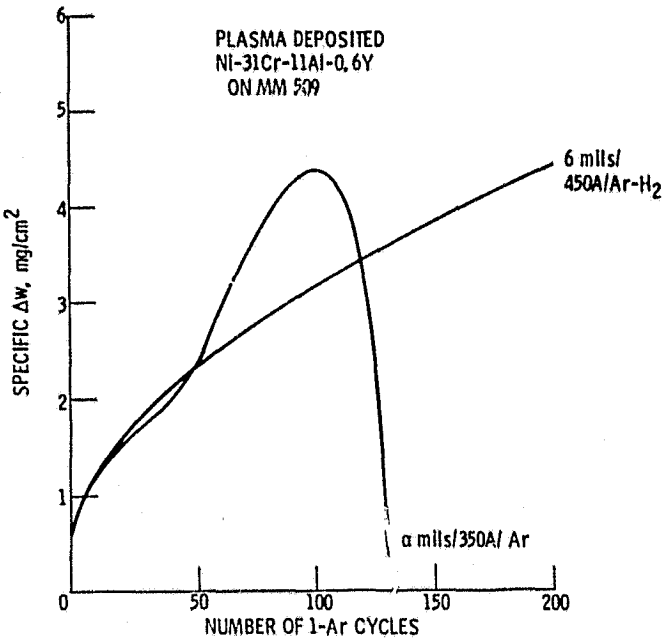

Figure 26. - Effect of coating depostion parameters on 2012° F oxidation.

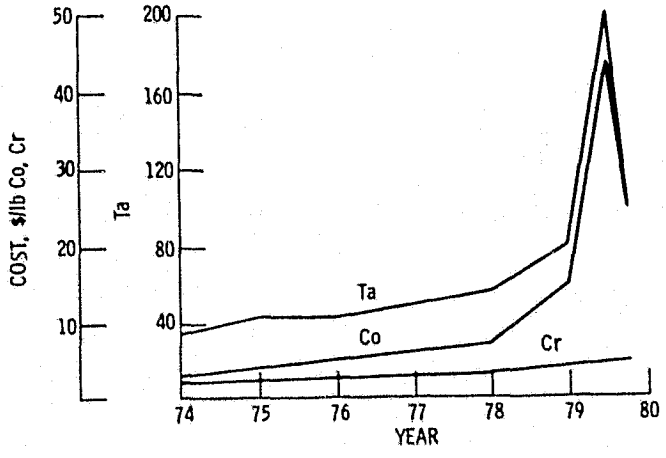

Figure 27. - Price of scarce metals.

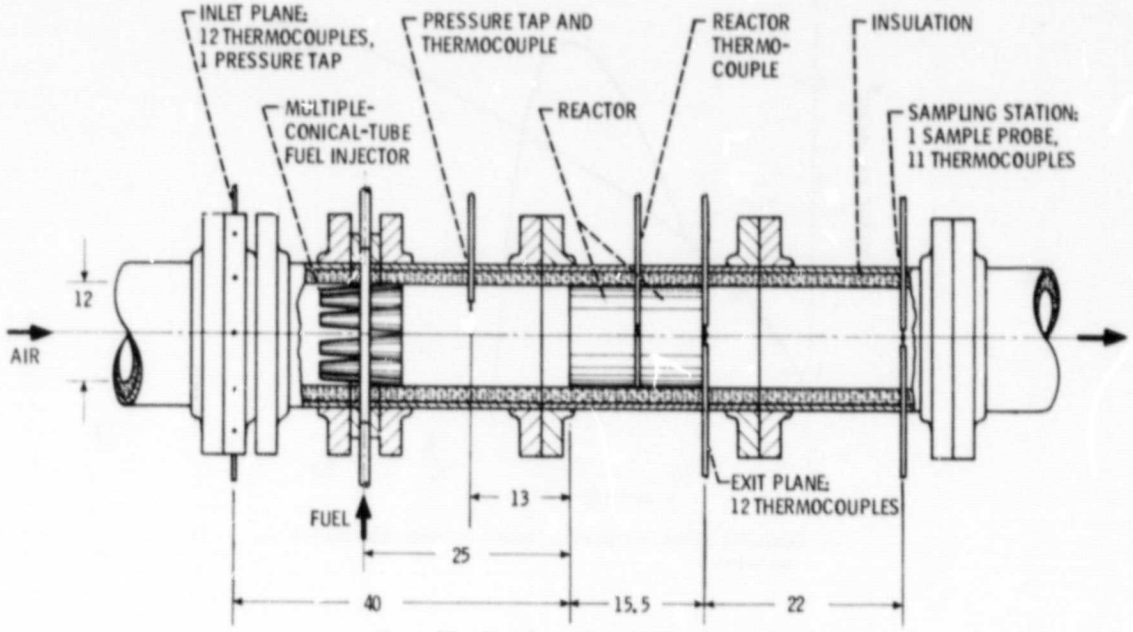

Figure 28. - Experimental apparatus. (Dimensions in cm.)

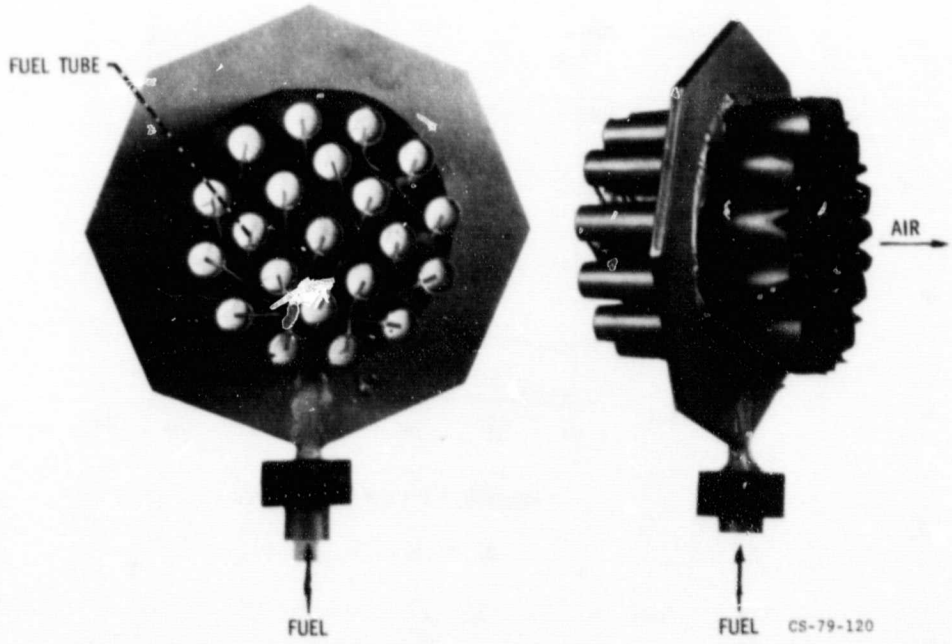

Figure 29. - Multiple conical tube fuel injector.

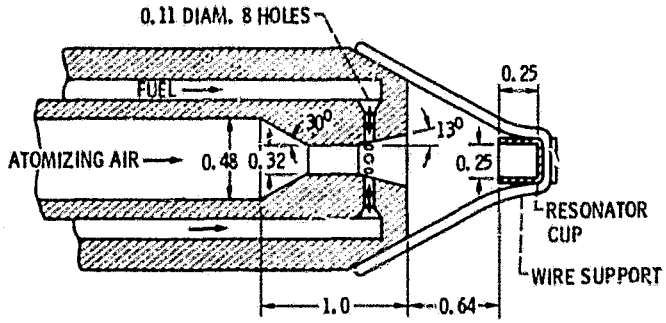

Figure 30. - Sonicore fuel injector (Dimensions in cm).

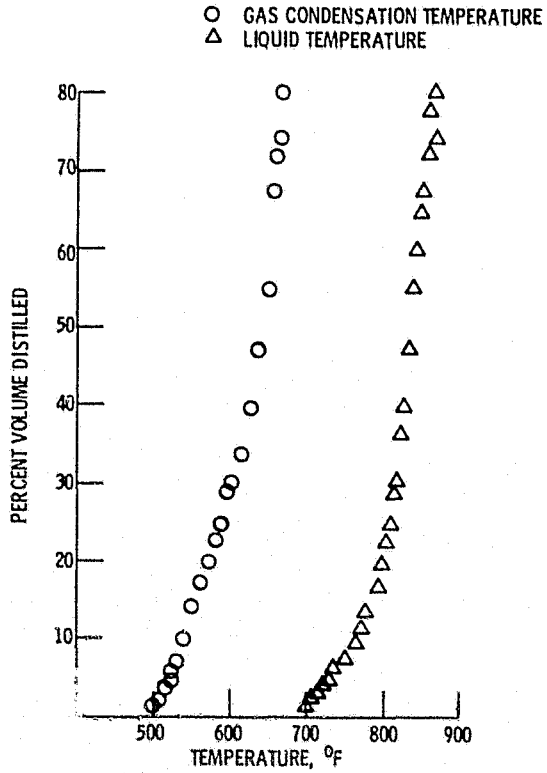

Figure 31. - Atmospheric distillation of bunker C fuel.